The Thesis committee for Khai Yi Chin
Certifies that this is the approved version of the following thesis:

Molecular Doping of Carbon Nanotube Conductors

APPROVED BY

SUPERVISING COMMITTEE:

Eric Fahrenthold, Supervisor

Michael Cullinan

Molecular Doping of Carbon Nanotube Conductors

by

Khai Yi Chin

THESIS

Presented to the Faculty of the Graduate School of

The University of Texas at Austin

in Partial Fulfillment

of the Requirements

for the Degree of

Master of Science in Engineering

THE UNIVERSITY OF TEXAS AT AUSTIN

May 2018

Acknowledgments

I owe my deepest gratitude to my advisor Dr. Eric Fahrenthold, who provided endless support and experienced insights during the course of my research. This thesis would not have been possible without his leadership and patience in his guidance.

I would like to express my thanks to my father, Shyi Her Chin, my mother, Pik Choo Peng, and my siblings for their unwavering support of my academic and professional development in the United States.

I would like to show my gratitude to my friends and colleagues for their continued moral support.

This work was supported by the Office of Naval Research grant (Grant No. N00014-15-1- 2693). Computer time support provided by the Texas Advanced Computing Center at the University of Texas at Austin and the Department of Defence High Performance Computing Modernization Program.

Molecular Doping of Carbon Nanotube Conductors

Khai Yi Chin, MSE
The University of Texas at Austin, 2018

Supervisor: Eric Fahrenthold

Carbon nanotubes (CNTs) show attractive electronic properties that have been studied extensively, including interest for cabling and wiring applications. Specifically, CNTs may provide an advantage over conventional materials, such as copper, due to their lightness and flexibility, which are properties demanded in naval and aircraft applications. Using molecular doping with the potassium tetrabromoaurate molecule ($KAuBr_4$), doped nanowires with enhanced electrical properties may be obtained. This thesis presents the first comprehensive modeling effort on $KAuBr_4$ doping of CNTs, including doping of SWNT junctions.

The results showed that the dopants had an overall positive effect on SWNT based conductors. The conductance of K doped junctions was similar, regardless of doping configuration, while the conductance for the $AuBr_4$ doped junction was heavily reliant on the doping configuration. The $AuBr_4$ doping fragment showed a unique characteristic: it eliminated the dependence of the junction conductance on nanotube overlap. A nanowire model was developed

and used as a metric for comparison with experimental studies of $KAuBr_4$ doped CNTs. The nanowire model provided a reasonable comparison of the computational results with previous experimental work. Overall, results presented in this thesis show the promise of doped SWNTs as potential candidates for the replacement of conventional copper conductors.

Table of Contents

List of Tables

List of Figures

Chapter 1

Introduction

Carbon nanotubes (CNTs) have attracted much attention since physicist Sumio Iijima identified hollow cylindrical carbon structures in 1991 [1]. Since then, research on the material has escalated in order to study its unique properties. In particular, the electronic properties of CNTs show great promise, and provide an attractive prospect for applications like power transmission and consumer electronics. Specifically, conventional materials used in electrical applications, such as copper, are heavy and have poor mechanical properties; CNT-based wires may be able to resolve those complications with superior mechanical and electrical properties [2]. Recent research showed the advantage of doped CNT cables over conventional copper cables in terms of specific conductivity [3]; another paper showed a flexible and conductive CNT-based electrode [4]. This work on doped CNTs can contribute to the fabrication of highly conductive nanotubes in many of these applications.

In order to replace conventional conductive materials, the enhancement of electrical conductivity in CNTs is a highly reseached topic. One way of enhancing the electrical conductivity is through the chemical doping of the CNTs. Some experimental studies of doped CNTs include I_2, ICl, IBr [5],

$KAuBr_4$ [6, 7], K, Br [8], and $AuCl_3$ doped [9] CNTs.

Zhao et al. [3] showed a very high specific conductivity in iodine doped CNTs, which a previous work studied its computational models [10]. Similarly, motivated by recent experimental efforts where CNT wires doped in a $KAuBr_4$ aqueous solution show high conductivity over undoped CNT wires [6, 7], this thesis explores the effect of potassium tetrabromoaurate ($KAuBr_4$) on single-walled nanotube (SWNT) conductors and junctions. (In this thesis, the $KAuBr_4$ investigated has a gold oxidation number of +3, represented by the Roman numeral III [11].) Notably, the doped CNT wires showed increased conductivity, but decreased specific conductivity (specific conductivity is defined in a continuum as σ/ρ, where σ is the conductivity, and ρ is the mass density, of the continuum). No computational work on $KAuBr_4$ as a CNT dopant was found at the time of this writing. Furthermore, the possibility of the $KAuBr_4$ molecule disassociating is considered, since the exact chemical makeup of the doped CNT is unknown. In this thesis, both the K atom and $AuBr_4$ fragment were included as potential dopants in the analysis.

K doping has been shown to improve the SWNT conductivity as well as its high-temperature stability (the change in conductivity was low across a wide range of temperatures) [8]. In that cited work however, the K doping process was limited to a small sample size; the procedure involved transferring the reacted sample into a cryostat, which limits the yield. This poses an obstacle for the fabrication of conductive wires, since a high volume of these wires is required. Alternative K doping methods have been found, however:

K doped multi-walled nanotubes were produced through a reaction with a phenanthrene/K solution [12], which allows doping of larger volumes of CNTs. Moreover, the electronic structure of K doped SWNTs were investigated computationally [13]. In that work, the K atoms were positioned in the center of semiconducting SWNT conductors without structural relaxation. The researchers observed an upwards shift of the Fermi energy in the band structure, which is an indication of the n-doping of nanotubes by the K atoms. A different doping configuration for the K atoms is shown in this thesis, for both the SWNT conductor and junction models.

The $AuBr_4$ fragment was not studied as a dopant for CNTs, but results on a similar dopant ($AuCl_3$) exist. Kim et al. found a decrease of sheet resistance in $AuCl_3$ doped CNT films with increasing dopant concentration, undergoing a decrease as much as 90% with an $AuCl_3$ concentration of 60 mM [9]. A further study using Raman and x-ray photoelectron spectroscopy showed that the element chlorine, rather than the gold, in the $AuCl_3$ molecule is responsible for the p-doping of the CNT, thus reducing the sheet resistance [14]. More recently, a computational study determined that it was neither the Cl nor the $AuCl_3$ (and Au_2Cl_6) that induced the p-doping, but the $AuCl_4$ [15]. Building upon that result, $AuCl_4$ doped conductors have been studied computationally and found to improve the conductance of the SWNT [16], but there were no computational studies on $AuBr_4$ doped SWNTs at the time of writing. In this work, that gap in knowledge will be bridged through the investigation of $AuBr_4$ doped SWNT conductors and junctions.

Apart from the neutral K atom and $AuBr_4$ fragment, their charged counterparts were modeled as well, namely, the K^+ and $AuBr_4^-$ ion. The modeling of the charged dopants was motivated by the uncertainty in the doping configuration presented in [6, 7]: the doping solution used to produce the $KAuBr_4$ doped CNT in the two works was a $KAuBr_4$ aqeuous solution, which raised the possibility of K^+ and $AuBr_4^-$ as doping agents in the solutions. Hence the effect of charged dopants on SWNT conductors was investigated in this research. There were no published experimental measurements on the doping configurations for the $KAuBr_4$ solution, thus the results in this thesis show several possible cases ($KAuBr_4$, K, $AuBr_4$, K^+, and $AuBr_4^-$) which may result from said doping solution.

In terms of SWNT junctions, Li and Marzari looked at (5,5) nanotube junctions and showed the potential of transition metals as a 'linker' atom in the junction interface, to improve the electrical conductance of the junctions [17]. Their junction models only considered transition metals as dopants, and only had about a one half unit cell of junction overlap. Saito studied the computational model of packed K doped CNT arrays as a candidate for superconductors [18], and observed an upwards shift in the Fermi energy, a sign of n-doping. K doped junctions in this thesis are different, in that multiple overlap distances were considered, and the junctions have only two end electrodes (this means that electronic transport from one end to another is more likely to be due to intertube travel as compared to arrays of complete SWNT conductors).

The closest computational study to $AuBr_4$ doped junctions were $AuCl_4$ doped junctions [16], but the junction models presented in that work utilized four terminals (electrodes), and the tube axes of the SWNTs were orthogonal to each other, which differs from the junction models presented in this thesis. In that work, they utilized (10,0) semiconducting SWNT junctions, and showed an increase of conductance from zero to an ideal metallic SWNT conductance. In this thesis, the $AuBr_4$ doped junctions presented are of metallic SWNTs; the dependence of conductance on dopant configuration is shown as well.

To limit the scope of this work, only two types of SWNTs were studied: the armchair SWNT of chirality (5,5) is the representative metallic SWNT, while the zigzag SWNT of chirality (8,0) is the representative semiconducting SWNT, both initialized as a rolled graphene sheet. Even so, the results obtained here are expected to be similar for the other metallic and semiconducting SWNTs; in the future, a set of dissimilar SWNTs should be considered for investigation. The transport calculations for the conductors were done to replicate the conductance of an isolated SWNT. As for the junctions, the transport calculations were done to simulate a macro-scale wire packed with SWNTs, in order to simulate the conditions similar to the experimental work in [7], where the CNT wires were fabricated through radial densification. That was done through the placement of a SWNT junction model in a computational unit cell that defines the packing of the junctions. For the doped SWNT junctions, two configurations are shown: the external doping and the interstitial doping

configuration. The variety in configurations addresses the effect of doping distribution on junction conductance, which was shown in a previous work on a detailed look at dopant distribution using iodine doped SWNTs [10]. The configuration of the dopants (in the experiment) for a $KAuBr_4$ doping solution is not known. It is likely that the solution contains some mixture of K atoms and $AuBr_4$ fragments. New experimental methods would be needed to explicitly control dopant configurations, which was not shown in the aforementioned experimental works [6, 7].

Besides dopant dependent conductance effects, other influences in the SWNT junction models were also studied. The conductance of the junction is a complex subject that can be affected by: SWNT tube axis alignment [19], interface alignment (stacking alignment in graphene junctions) [20–23], overlap distances (SWNT and graphene) [19,23], intertube separation distance (graphene nanoribbon-graphene interlayer distance) [24]. The effects of SWNT rotational configuration, overlap distances, and nanotube separation distances (packing arrangement) on the junction conductance are discussed here.

The thesis is organized as follows: Chapter 2 discusses the methodology used in investigating the models, Chapter 3 presents results on SWNT conductors, while Chapter 4 shows the results on SWNT junctions. In addition, a nanowire model was proposed to scale the SWNT results and determine specific conductivity. Chapter 5 presents the nanowire model and compares it with a benchmark material, copper. Conclusions on the presented results are drawn in Chapter 6. Finally, in Appendix A, the results on the ion doped

SWNT conductors are presented.

Chapter 2

Methodology

Structural relaxation for all presented models was performed using the SIESTA 4.0 computational package, a self-consistent density functional theory (DFT) software that uses a basis set based on linear combinations of atomic orbitals (LCAO) [25]. In all cases, the atomic orbitals were double-ζ polarized. Exchange-correlation functionals were obtained using the Generalized Gradient Approximation (GGA) method, parametrized by Perdew, Burke, and Ernzerhof (PBE) [26], matched with an orbital energy shift $\Delta E_{PAO} = 150$ meV [27]. The k-grid mesh for structural relaxation was $1 \times 1 \times 1$, while the k-grid mesh for transport calculations was $1 \times 1 \times 4$. The relatively coarse mesh [16, 28] was selected due to the size of the computational models; a finer mesh ($1 \times 1 \times 4$ for structural relaxation) was tested; it was found that the difference in results was negligible ($< 2\%$), while the computation time was much longer (four times as long). The mesh cutoff energy was 300 Ry for both the structural relaxation and transport calculations [28]. For ab-initio computations, bonds do not exist; the "bonds" shown in this work represent the electrostatic forces between atoms. Dispersion correction was not incorporated in the calculations of this thesis, since there have been DFT studies that showed accurate SWNT band gap values without dispersion correction [29].

However, dispersion corrected models are of interest in future studies.

A computational unit cell (used to specify a packing arrangement) under periodic boundary conditions was used for the relaxation and transport calculations. All models were relaxed until the maximum atomic force in the system was less than 0.04 eV Å^{-1}.

Transport calculations were performed with the TranSIESTA module included in the SIESTA 4.0 package, which computes the charge density matrix using Green's functions [30]. The conductance G is expressed in the form of the multichannel Landauer conductance formula [31, 32]:

$$G = G_0 \int \left(-\frac{\partial f(E)}{\partial E} \right) T(E) dE, \; T(E) = \text{Tr}[t^\dagger(E) t(E)], \tag{2.1}$$

where Tr is the trace operator, $t(E)$ is the transmission matrix, † is the conjugate transpose operator, $\text{Tr}[t^\dagger(E)t(E)]$ is the transmission amplitude at energy E, $f(E)$ is the Fermi-Dirac distribution, and the conductance quantum is

$$G_0 = \frac{2e^2}{h} = 7.748 \times 10^{-5} \text{ S}, \tag{2.2}$$

where e is the elementary charge, and h is Planck's constant. All results presented in this work were computed at zero temperature conditions, and thus Eqn. (2.1) becomes [31]

$$G = T(E_F) G_0. \tag{2.3}$$

In order to perform the transport calculations, each model was split into three regions: two end electrodes (one on each end) and the central scattering region.

The end electrodes used in all calculations are extensions of the central scattering region, i.e., they are of the same species and configuration, instead of a different element (e.g. gold electrodes with a SWNT central scattering region). This is because of the intention is to simulate macro-scale CNT conductors, which can be approximated as infinitely long. Furthermore, the inclusion of buffer atoms is required when using bulk electrodes of a different species, which will further enlarge the model size and prolong the computation time. The electrodes range from 2 to 4 unit cells in length, depending on the model and dopant size, and are semi-infinite: they extend to infinity on ends that are not connected to the scattering region, via periodic images.

Chapter 3

Conductor Models

The investigation of $KAuBr_4$ doped CNTs began with the modeling of SWNT conductors. Through the conductor models, the effects of different dopants on the conductance (a measure of effectiveness in intratube electronic movement) was observed. Motivated by the experimental efforts of $KAuBr_4$ doped CNTs [6, 7], a $KAuBr_4$ dopant was chosen in an attempt to shed light on the mechanism behind the improvement of the electrical conductivity of the nanotubes. As the exact dopant standoff and dopant type were unknown, the possibility of the K atoms and $AuBr_4$ fragments disassociating from their $KAuBr_4$ form in the doping solution was considered. Hence, the conductance of the undoped, $KAuBr_4$ doped, K doped, and $AuBr_4$ doped SWNT conductors is presented in this chapter.

Prior to transport calculations, structural relaxation was performed on all the models. The SWNT conductors were relaxed in an isolated environment, i.e., the undoped/doped conductors were relaxed in a large computational unit cell to prevent interactions between the periodic images. The SWNT conductors modeled are 20 Å away from the walls in the x- and y-directions, while the z-walls were positioned such that the periodic images of

the computational unit cell simulate a continuous and infinitely long SWNT conductor. Once relaxed, transport calculations were carried out on the SWNT conductor models in the same computational unit cell.

As mentioned in Chapter 1, there is a great interest in the specific conductivity of the doped models, in addition to the conductance. In the conductor models, the transport calculations were performed with two isolated nanotubes; as such, the volume of the conductor models was not considered. Therefore, the results of conductance and specific conductance (instead of specific conductivity) of the modeled SWNT conductors are computed. The specific conductance of the conductors is defined by:

$$\hat{G}_c = \frac{G_c}{\hat{m}_c},\ \hat{m}_c = \frac{m_c}{L_c} \tag{3.1}$$

where G_c is the conductance of a SWNT conductor with mass per unit length of $\hat{m}_c$, L_c is the unit cell length of the conductor, and m_c is the unit cell mass of the conductor. The atomic masses of the different elements considered are listed in Table 3.1, obtained from [33].

The SWNT conductors were modeled with two different dopant concentrations; the concentration values depend on the dopant species. (Note that in this thesis, dopant concentration is referred to as the number of atoms/fragments/molecules of dopants per SWNT unit cell; Table 3.2 tabulates the dopant mass fractions for the different dopants, and the dopant concentrations.

The dopants were initialized at a distance of 1-1.1 Å from the nanotube

surface, which was sufficient to induce inter-atomic interactions; in all the cases, the dopants relaxed to a distance further away from the initial position, shown in Table 3.2 as dopant standoff ($l^*_{dopant-SWNT}$).

3.1 Undoped Conductors

The SWNTs were initialized as a rolled graphene sheet with a carbon-carbon bond length of 1.42 Å, leading to diameters of 6.26 Å and 6.78 Å respectively for the (8,0) SWNT and the (5,5) SWNT, which match literature values [34]. In terms of band structures, the models are consistent with past work [29,34]: the (8,0) SWNT has a band gap of 1.25 eV and the (5,5) SWNT has a zero band gap, both shown in Fig. 3.1.

For the undoped cases, the (8,0) SWNT conductor has a conductance of zero at the Fermi energy E_F, while the (5,5) SWNT conductor has a conductance of $2G_0$ at E_F. These results match literature values [35, 36]. The mass per unit length for the undoped (8,0) SWNT is 90.160 amu Å^{-1}; similarly 97.601 amu Å^{-1} for the (5,5) SWNT.

3.2 Potassium Tetrabromoaurate Doped Conductors

The first doped SWNT conductor model studied was the $KAuBr_4$ doped conductor. The $KAuBr_4$ molecule spans the length of two unit cells in the (8,0) SWNT, and three unit cells in the (5,5) SWNT, shown in Figs. 3.2 and 3.3. Hence, the $KAuBr_4$ dopant concentrations tested are 0.50 and 1.00 molecules

per unit cell for the (8,0) SWNT. Correspondingly, the dopant concentrations are 0.33 and 0.67 molecules per unit cell for the (5,5) SWNT. The dopant standoff, the doped mass per unit length, and the dopant mass fraction are listed in Table 3.2.

The $KAuBr_4$ molecule had no effect on the conductance of the (8,0) SWNT, which remained at zero at both dopant concentrations. However, the conductance of the (5,5) SWNT increased with increasing dopant concentration, almost doubling to $3.98G_0$ at the higher concentration. Despite this effect, the specific conductance was not improved, due to the high mass of the $KAuBr_4$ molecule, as shown in Fig. 3.4. The equilibrium geometry of the dopant molecule differed between the $KAuBr_4$ doped (8,0) SWNT and the $KAuBr_4$ doped (5,5) SWNT, as shown in Figs. 3.2 and 3.3 respectively. In the (8,0) SWNT case, the K atoms in the $KAuBr_4$ molecule aligned into a single plane, whereas in the (5,5) SWNT case the K atoms moved away from the plane of the $AuBr_4$.

The $KAuBr_4$ has been shown to improve the conductivity of CNTs [7], consistent with the present work, noting that bulk SWNTs include both metallic and semiconducting nanotubes [37].

3.3 Potassium Doped Conductors

The second dopant considered was the K atom, disassociated from its $KAuBr_4$ form. The K atom spans the length of one unit cell in both the (8,0) and (5,5) SWNT conductors, as shown in Figs. 3.5 and 3.6. Hence, the dopant

concentrations are 0.50 and 1.00 atoms per unit cell for both the (8,0) and (5,5) SWNT. The dopant standoff, the doped mass per unit length, as well as the dopant mass fraction are listed in Table 3.2.

The K doping had a very positive effect on conductance for both the (8,0) and (5,5) SWNT conductors. At the dopant concentration of 1.00 atoms per unit cell, the conductance increased to pass the benchmark value for an undoped (5,5) conductor: $2G_0$. Due to the low mass of the K atom, the specific conductance for both types was also improved, as shown in Fig. 3.7. Band structure analysis, shown in Figs. 3.11(left) and 3.12(left), showed that there was an upwards shift in the Fermi energy, a sign of the n-doping of the SWNT conductor by the K atom. This led to an increase in electronic states available near the doped Fermi energy, and consequently an improvement in the conductance. The results are qualitatively consistent with experiment, where the potential of potassium atoms to improve the conductivity of SWNTs is shown [8].

3.4 Tetrabromoaurate Doped Conductors

The third dopant investigated was the $AuBr_4$ fragment, the other disassociated part of the $KAuBr_4$ molecule. The $AuBr_4$ fragment spans the length of two unit cells in the (8,0) SWNT conductor, and three unit cells in the (5,5) SWNT conductor, as shown in Figs. 3.8 and 3.9. Hence, the $AuBr_4$ framgent concentrations tested are 0.50 and 1.00 fragments per unit cell for the (8,0) SWNT conductor. The dopant concentrations are 0.33 and 0.67 fragments per

unit cell for the (5,5) SWNT conductor. The dopant standoff, the doped mass per unit length, and the dopant mass fraction are listed in Table 3.2.

The $AuBr_4$ doping improved conductance for both the of SWNT conductors, especially for the (5,5) conductor, shown on the left of Fig. 3.10. Band structure analysis, shown in Figs. 3.11(right) and 3.12(right), showed that there was a downwards shift in the Fermi energy, a sign of p-doping of the SWNT conductor by the $AuBr_4$ fragment. This led to an increase in electronic states available near the doped Fermi energy, and consequently an improvement in the conductance. It is qualitatively consistent with the closest experimental work related to $AuBr_4$ doping, which is the $AuCl_3$ doping of CNT films [9]. In that work the authors observed a decrease in sheet resistance of the doped film over its undoped counterpart.

Given the mass of the $AuBr_4$ fragment, the specific conductance remains below the benchmark value for an undoped metallic (5,5) SWNT, as shown on the right of Fig. 3.10.

3.5 Summary of Results: SWNT Conductors

The SWNT conductors had the following reaction to the dopants:

- $KAuBr_4$: The $KAuBr_4$ molecule had mixed effects on the conductance of the SWNT devices. The (8,0) conductor was unaffected by the $KAuBr_4$ dopant: its conductance remained at zero. The (5,5) conductor showed an increase in conductance with $KAuBr_4$ doping: the conductance raised

from $2G_0$ to $3G_0$ at 0.33 molecules per unit cell, and to $4G_0$ at 0.67 molecules per unit cell. The specific conductance of the (8,0) conductor was zero (since the $G = 0$), while the $KAuBr_4$ doping reduced the specific conductance of the (5,5) conductor, despite a significant improvement to the conductance. The dopant mass fraction for the $KAuBr_4$ was very large, going as high as 60% and 61% for the (8,0) and (5,5) conductors respectively. The relaxed configuration of the $KAuBr_4$ molecule differed between the two types of SWNT conductors, which suggested that the full-planar configuration of the $KAuBr_4$ molecule reduces conductance in the (8,0) SWNT, while the separated K atom and $AuBr_4$ fragment improve conductance; the effects of the disassociated parts are also shown in this chapter.

- K: The K atom had a positive effect on both the (8,0) and the (5,5) conductors. The (8,0) conductor saw an increase in conductance: the conductance increased from 0 to $1.6G_0$ at 0.50 atoms per unit cell, and to $2.5G_0$ at 1.00 atoms per unit cell. The (5,5) conductor also saw an increase in conductance: the conductance increased from $2G_0$ to $3G_0$ at 0.50 atoms per unit cell, and to $3.8G_0$ at 1.00 atoms per unit cell. The specific conductance of the (8,0) conductor was increased, going over the benchmark value of an undoped (5,5) SWNT at 1 atoms per unit cell, while the specific conductance of the (5,5) conductor exceeded the same benchmark at 0.50 and 1.00 atoms per unit cell. Since the K atom is relatively light, the dopant mass fraction was low for both

semiconducting and metallic SWNT conductors, going only as high as 9% for the (8,0) conductor and 14% for the (5,5) conductor. From the band structure analysis, the increase in conductance is attributed to n-doping of the SWNT conductor by the K atom.

- $AuBr_4$: The $AuBr_4$ dopant had a positive effect on both the (8,0) and the (5,5) conductors. The (8,0) conductor saw an increase in conductance: the conductance increased from 0 to $1.3G_0$ at 0.50 fragments per unit cell, and to $1.9G_0$ at 1.00 fragments per unit cell. The (5,5) conductor also saw an increase: the conductance increased from $2G_0$ to $3G_0$ at 0.33 fragments per unit cell, and to $0.67G_0$ at 0.67 fragments per unit cell. However, the specific conductance of both the (8,0) and (5,5) conductors were lower than the benchmark value for the undoped (5,5) SWNT. Since the $AuBr_4$ fragment is heavy, the dopant mass fraction was high for both the semiconducting and metallic SWNT conductors, going as high as 57% for the (8,0) conductor and 59% for the (5,5) conductor. From the band structure analysis, the increase in conductance is attributed to p-doping of the SWNT conductor by the $AuBr_4$ fragment.

The results for the ion dopants are shown in Appendix A. The conductance of the ion-doped conductors was not affected: for the (8,0) SWNT conductor $G = 0$, and for the (5,5) SWNT conductor $G = 2G_0$. The specific conductance remained at zero for the ion doped (8,0) conductor, while the specific conductance decreased slightly for the ion doped (5,5) conductor. The

dopant mass fraction for each ion dopant was the same as its charged counterpart, shown in Table 3.2. Table A.1 lists the dopant standoff, mass per unit length, and conductance for the ion doped conductors.

Table 3.1: Atomic masses of atoms used in models.

Element	K	Au	Br	C
Mass (amu)	39.098	196.967	79.904	12.012

Table 3.2: Dopant standoff (from SWNT surface), mass per unit length, and dopant mass fraction for the doped conductors.

Dopant	SWNT Chirality	Concentration (number /u.c.)	Dopant Standoff $l^*_{dopant-SWNT}$ (Å)	Mass per Unit Length $\hat{m}_c$ (amu Å^{-1})	Dopant Mass Fraction (%)
$KAuBr_4$	(8,0)	0.50	3.375 (Au)	155.3	0.420
		1.00	3.313 (Au)	220.5	0.591
	(5,5)	0.33	3.364 (Au)	172.9	0.435
		0.67	3.362 (Au)	248.1	0.607
K	(8,0)	0.50	2.352	94.7	0.048
		1.00	2.492	99.3	0.092
	(5,5)	0.50	2.618	105.6	0.075
		1.00	2.549	113.5	0.140
$AuBr_4$	(8,0)	0.50	3.382 (Au)	150.8	0.402
		1.00	3.186 (Au)	211.3	0.573
	(5,5)	0.33	3.507 (Au)	167.6	0.418
		0.67	3.375 (Au)	237.5	0.589

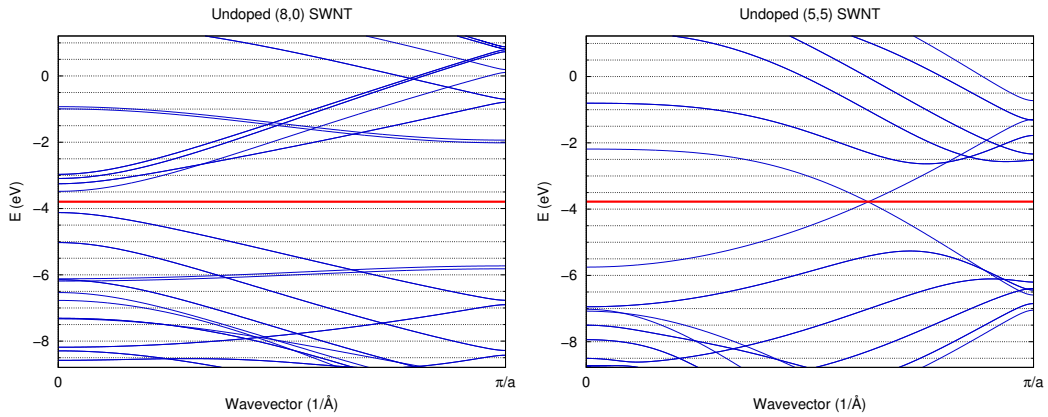

Figure 3.1: The undoped band structures of the (8,0) SWNT conductor (left), and the (5,5) SWNT conductor (right); the red line indicates the Fermi level.

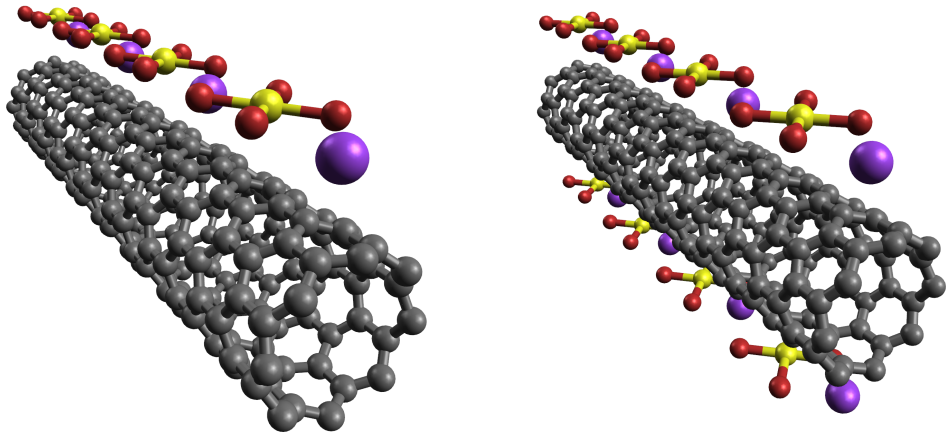

Figure 3.2: $KAuBr_4$ doped SWNTs: (8,0) SWNT with 0.500 dopant molecules per unit cell (left), and 1.000 dopant molecules per unit cell (right).

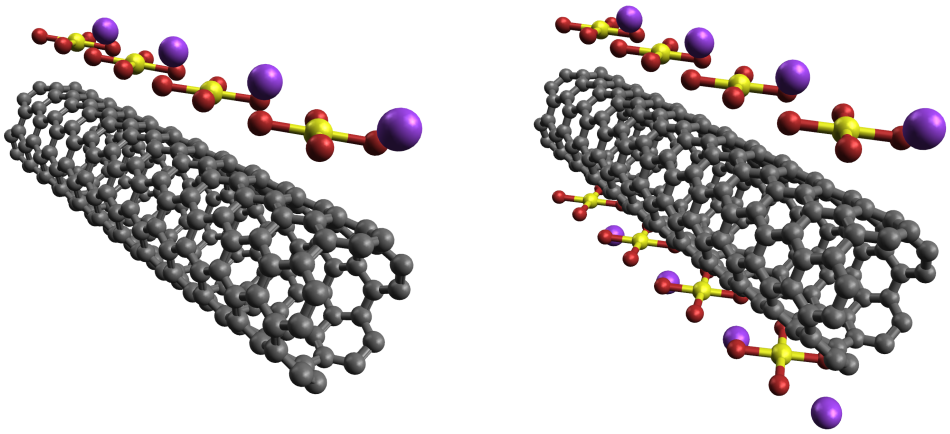

Figure 3.3: $KAuBr_4$ doped SWNTs: (5,5) SWNT with 0.333 dopant molecules per unit cell (left), and 0.667 dopant molecules per unit cell (right).

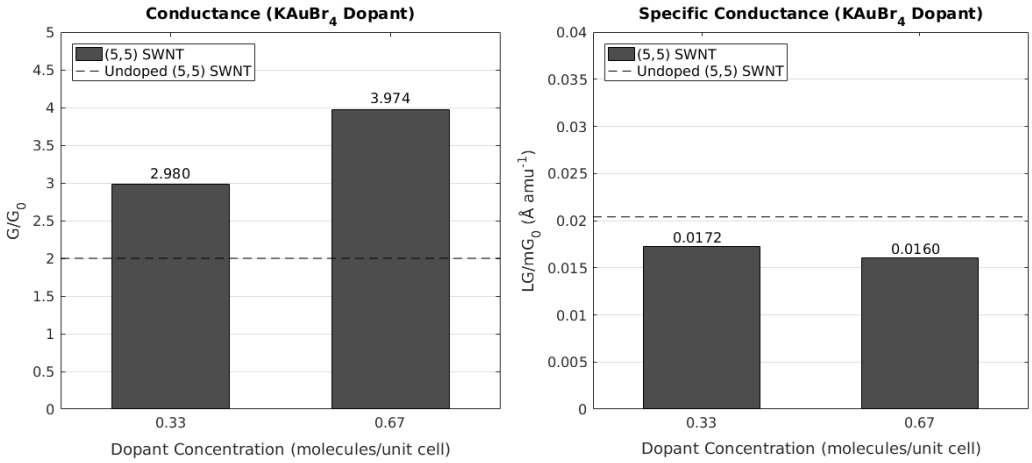

Figure 3.4: Performance of the $KAuBr_4$ doped SWNTs (conductance, left, and specific conductance, right), with the dashed lines representing an undoped (5,5) SWNT (note that the (8,0) SWNT was not affected by $KAuBr_4$ doping).

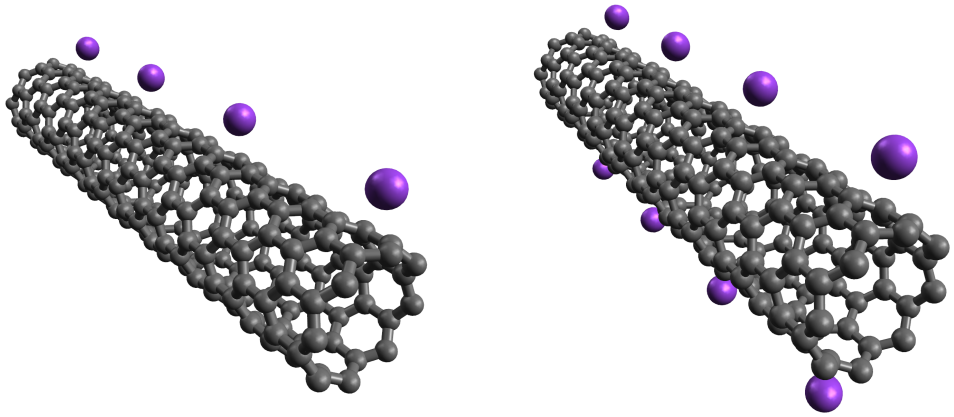

Figure 3.5: K doped SWNTs: (8,0) SWNT with 0.500 dopant atoms per unit cell (left), and 1.000 dopant atoms per unit cell (right).

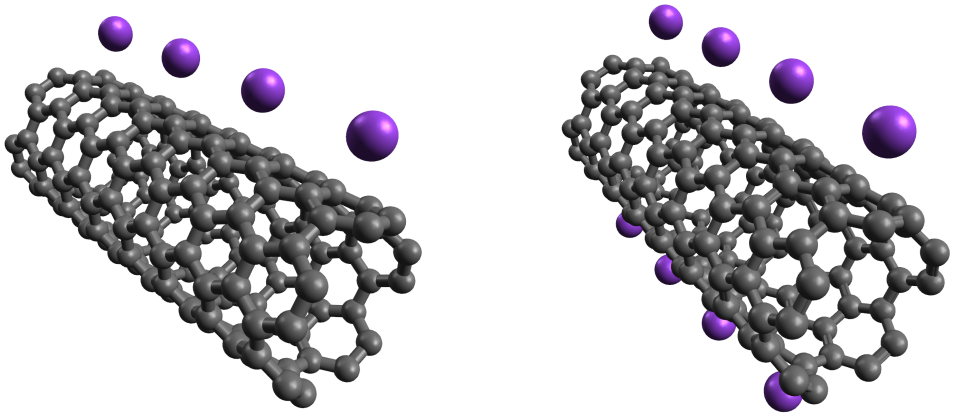

Figure 3.6: K doped SWNTs: (5,5) SWNT with 0.500 dopant atoms per unit cell (left), and 1.000 dopant atoms per unit cell (right).

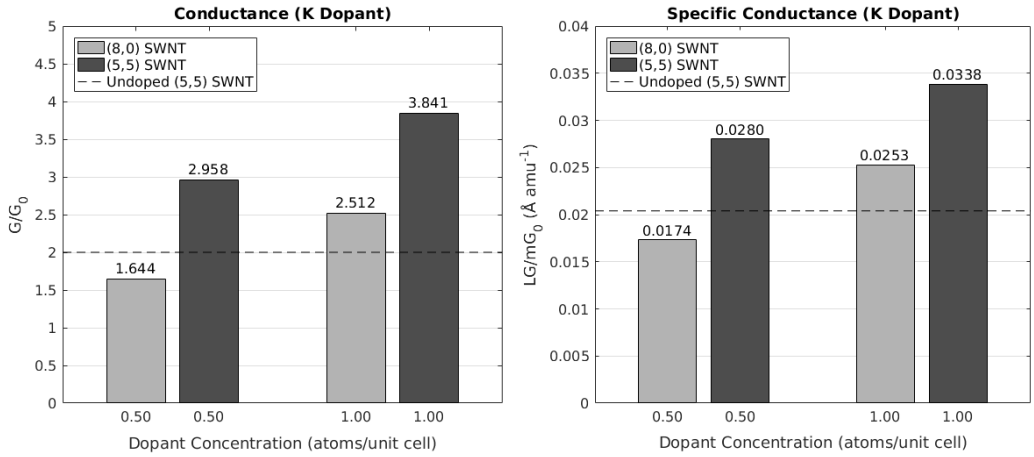

Figure 3.7: Performance of the K doped SWNTs (conductance, left, and specific conductance, right), with the dashed lines representing an undoped (5,5) SWNT.

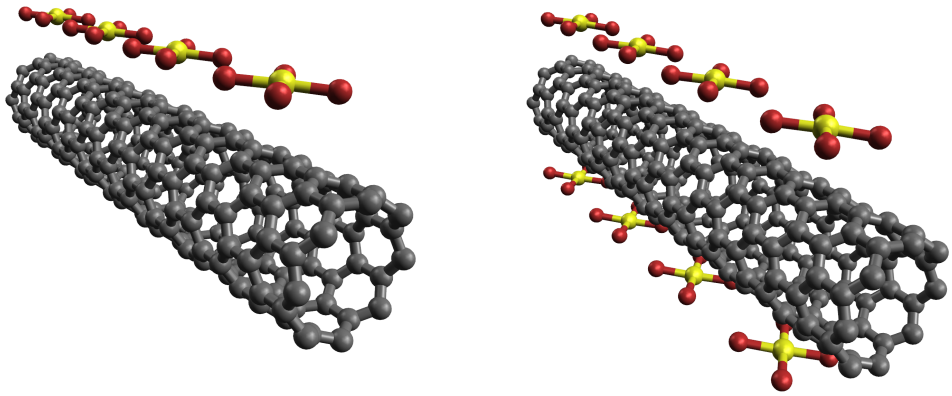

Figure 3.8: $AuBr_4$ doped SWNTs: (8,0) SWNT with 0.500 dopant fragments per unit cell (left), and 1.000 dopant fragments per unit cell (right).

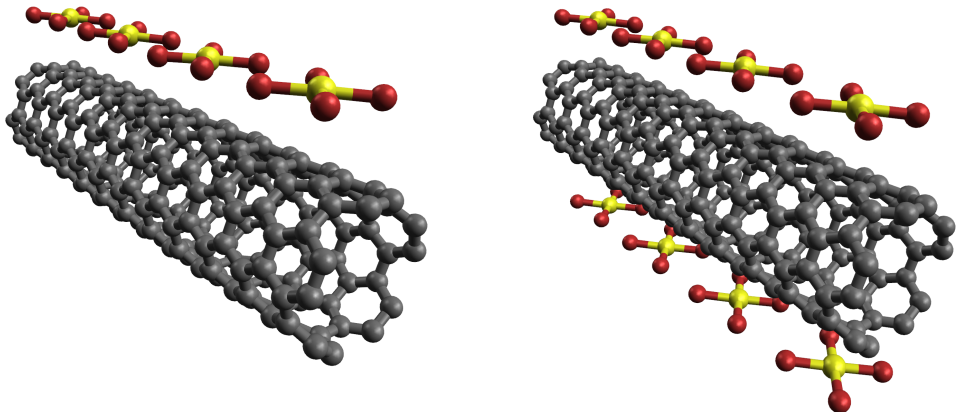

Figure 3.9: $AuBr_4$ doped SWNTs: (5,5) SWNT with 0.333 dopant fragments per unit cell (left), and 0.667 dopant fragments per unit cell (right).

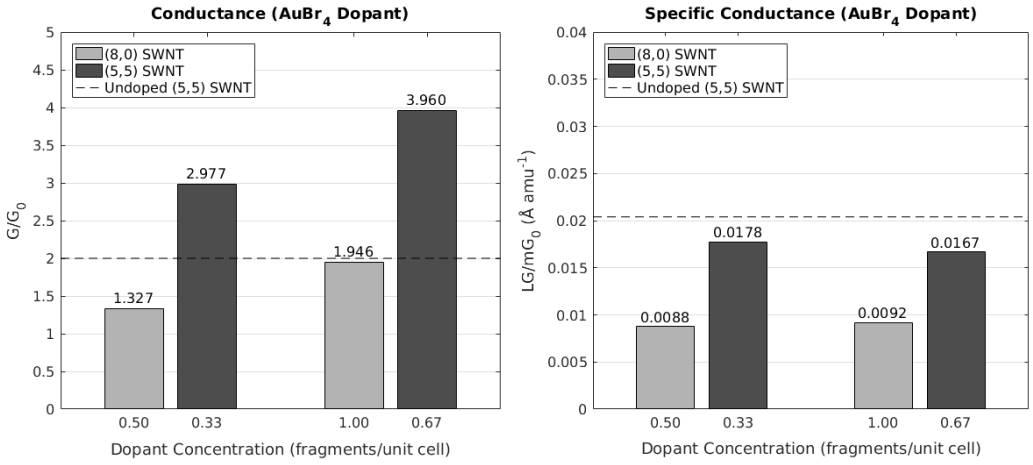

Figure 3.10: Performance of the $AuBr_4$ doped SWNTs (conductance, left, and specific conductance, right), with the dashed lines representing an undoped (5,5) SWNT.

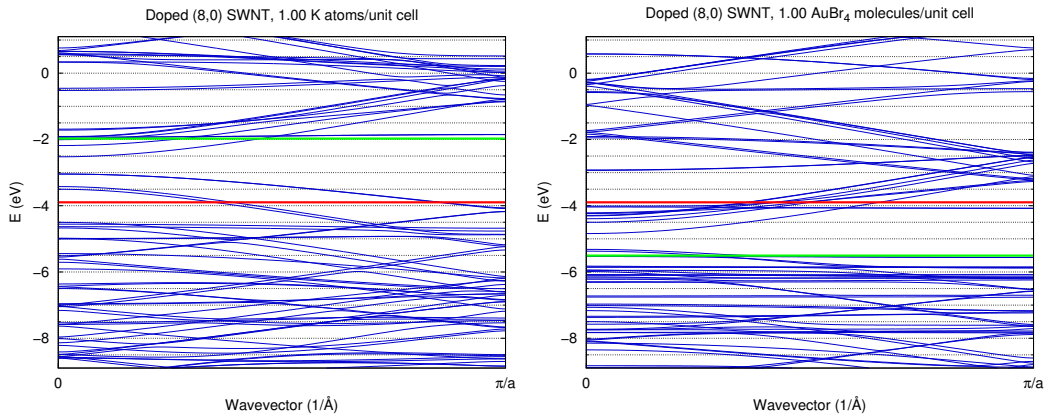

Figure 3.11: The doped (8,0) band structures of the K doped conductor (left), and the $AuBr_4$ doped conductor. The red line indicates the undoped Fermi level, while the green line indicates the doped Fermi level, for both doped conductors respectively. The shift in Fermi level and the bands show n-doping (left) and p-doping (right) of the SWNTs.

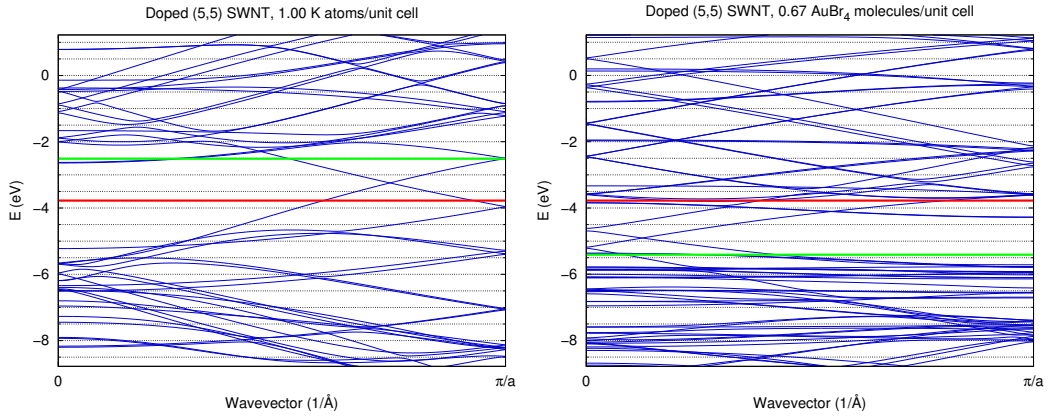

Figure 3.12: The doped (5,5) band structures of the K doped conductor (left), and the $AuBr_4$ doped conductor. The red line indicates the undoped Fermi level, while the green line indicates the doped Fermi level, for both doped conductors respectively. The shift in Fermi level and the bands show n-doping (left) and p-doping (right) of the SWNTs.

Chapter 4

Junction Models

Since any practical nanowire consists of a large number of noncontinuous CNTs, it is only rational to consider the intertube movement of electrons (in addition to the intratube conductance studied in Chapter 3), in order to better understand the conductivity of a macro-scale wire. To do this, SWNT junctions (which are models of one SWNT conductor end overlapping another conductor end) were simulated.

In this chapter results on the conductance of the SWNT junctions are shown. The (5,5) SWNT was chosen for the junction models because, as compared to the (8,0) SWNT, the metallic SWNT better allows observation of the doping effects. If the dopant is detrimental to the junction conductance, there would be a decrease in conductance (from $2G_0$), and if the dopant is beneficial, there would be an increase in conductance; in the case of the (8,0) SWNT, only the positive effects can be seen. Computational studies of metallic armchair junctions are scarce, especially for the dopants discussed in Chapter 3; no literature references could be found. The closest reference found investigated the doping effects of $AuCl_4$ on conductors and junctions [16], in which the junction was comprised of two semiconducting zigzag SWNTs. The work on the

metallic armchair SWNT junctions in this thesis will fill in a void pertaining to the conductance of doped metallic junctions, complementing the works on semiconducting SWNT junctions.

The K and $AuBr_4$ dopants were picked as a logical progression from the results obtained by studying the doped SWNT conductors. Notably, the K atom and the $AuBr_4$ fragments are reasonable disassociation states for the $KAuBr_4$ molecule. In addition, both the K and $AuBr_4$ dopants are symmetric: the K atom being a sole atom, and the $AuBr_4$ fragment being square planar. This eliminated dopant orientation as a degree of freedom that the $KAuBr_4$ would otherwise introduce. K^+ and $AuBr_4^-$ were considered as well, but due to their lack of effect on the SWNT conductors only their charge neutral counterparts are discussed in this chapter. Research on semiconducting junctions and the $KAuBr_4$ molecule in the future can build on the results for metallic junctions, as well as the K and $AuBr_4$ doping results presented here.

Besides dopant effects, the effects of overlap distances, nanotube separation distances, rotational configuration/misalignment, and packing on the conductance of the (5,5) junctions are presented. These variables are shown to produce drastic changes in junction conductance.

The SWNT junctions were modeled to simulate a finite volume of a bulk CNT wire: first, two aligned SWNT conductors in a computational unit cell size similar that for the conductor cases (with 20 Å from the x- and y- walls) were relaxed, to obtain an equilibrium configuration for the model. Then, alternate ends of the two conductors were discarded, to form a junction with

only two electrode ends, which was then moved to a different computational unit cell for transport calculations. This was done to simulate an environment of packed SWNT junctions; that is the computational unit cell determines the packing density. Further elaboration on the end removal procedures for the undoped and doped junctions are provided in their respective sections below.

4.1 Undoped Metallic (5,5) Junction

The first SWNT junction model investigated was the undoped metallic (5,5) junction. After the structural relaxation of two aligned (and isolated) SWNT conductors, the equilibrium nanotube separation distance between the two conductors was obtained, defined as $l^*_{SWNT-SWNT}$. The ends of the undoped conductors were then removed in the model,as follows: alternate ends of the two relaxed conductors were removed (equal lengths) depending on the overlap distances desired. Next, the SWNT junction was packed into a computational unit cell of dimensions $x_{junc} \times y_{junc} \times z_{junc}$, defined as:

$$x_{junc} = l^*_{SWNT-SWNT} + d_{SWNT} \tag{4.1}$$

$$y_{junc} = 2l^*_{SWNT-SWNT} + 2d_{SWNT} \tag{4.2}$$

$$z_{junc} = \text{length of model} \tag{4.3}$$

where d_{SWNT} is the diameter of the SWNT conductor. Figure 4.2 shows the undoped junction model, in the computational unit cell used in the transport calculations, and Table 4.1 lists the dimensions.

The model of two aligned, undoped (5,5) SWNTs, each 15 unit cells

long, was relaxed to a nanotube separation distance of $l^*_{SWNT-SWNT} = 3.36$ Å. Figure 4.1 shows the undoped (5,5) SWNT junction with a five unit cell overlap. At this nanotube separation distance, the conductance for the different overlap distances is shown in Fig. 4.9.

Apart from allowing the two aligned SWNTs to move freely in the y-direction, which resulted in a nanotube separation distance of $l^*_{SWNT-SWNT} = 3.36$ Å, the effect which different packing arrangements have on the conductance of the junction was determined. This was done to simulate conditions in a recent work, whereby the researchers radially densified rolled CNT sheets before doping them in $KAuBr_4$ solution [7]. To do this, the nanotube separation distance was initialized to $l_{SWNT-SWNT} = 1.50$, 2.00, 2.50, 3.00, 3.50, and 4.00 Å for structural relaxation (the asterisk has been removed to indicate that the distances are no longer for isolated nanotubes, but for packed nanotubes). The packing arrangements were obtained using the rules shown in Eqns. (4.1), (4.2), and (4.3), except that $l^*_{SWNT-SWNT}$ is replaced by $l_{SWNT-SWNT}$.

Due to the highly constrained conditions which the packing arrangement imposed on the model, the relaxed structure for the two SWNTs at the nanotube separation distance of $l_{SWNT-SWNT} = 1.50$ Å and 2.00 Å did not maintain a uniform circular cross section, leading to an unrealistically high total energy value. As for the nanotube separation distance of $l_{SWNT-SWNT}$ 2.50, 3.00, 3.50, and 4.00 Å, the energy values of the junctions were very close to the energy value of the junction at $l^*_{SWNT-SWNT} = 3.36$ Å, the difference being $< 0.03\%$. For all overlap distances, the energy values of all six junc-

tions ($l_{SWNT-SWNT}$ = 1.50 - 4.00 Å) were higher than the energy value of the junction that was structurally relaxed as isolated nanotubes (that gave $l^*_{SWNT-SWNT}$ = 3.36 Å).

In Fig. 4.1 the conductance for the different nanotube separation distances is shown, where the highest conductance value for the three, five, and seven unit cell overlaps occurred at $l_{SWNT-SWNT}$ = 3.00 Å. For the one unit cell overlap the highest conductance occurred at 2.5 Å. Comparing to the junction with a separation distance of $l^*_{SWNT-SWNT}$ = 3.36 Å (and a looser packing arrangement) shown in Fig. 4.9, it can be seen that at a closer packing the junction conductance rose sharply. Moreover, the dependence of the conductance on the overlap distance had an nonmonotonic behavior, which is not surprising; computational efforts have shown oscillatory conductance variations for both graphene [23], and SWNT junctions (labeled as contacts in their work) [38], as a function of overlap distance.

While there have been previous efforts to study the effects on junction conductance of overlap distances and tube axis alignment [19], there has not yet been any computational research on the rotational alignment of nanotubes in junctions. Thus the effects of rotational misalignment between the SWNT conductors in the junctions was investigated. Figure 4.4 shows three rotational configurations of the two conductors in the junction model: (a) is the model used for all junction calculations: the carbon atoms of the two SWNT conductor surfaces facing each other align perfectly. The upper conductor may be rotated along its tube axis, as shown in (b) for a rotation of 12°, and (c) for a

rotation of 18°. The unrolled view of the misaligned models is shown in Fig. 4.5. The choice of 12° and 18° rotations was driven by the honeycomb lattice of the SWNTs: a 12° rotation moves a carbon atom (in the upper conductor) to the lowest point of the conductor (in the y-direction), and an 18° rotation moves it slightly more, such that the same carbon atom now defines a joint lowest point on the conductor. The bottom conductor was stationary for all cases.

Figure 4.6 shows the effect of the rotational misalignment on the conductance. Both rotations reduced the conductance drastically, as compared to the junction with no misalignment, as shown on the left in Fig. 4.6. In fact, the 12° rotation created a gap in the transmission plot similar to that of an undoped semiconducting SWNT conductor, as shown on the right in Fig. 4.6, leading to zero conductance at the Fermi energy. The 18° rotation models had a finite conductance, albeit much lower than the rotationally aligned junction.

In carbon nanotubes, the p_z orbitals of the carbon atoms interact with each other to form π orbitals, which are the main contributors to the conduction of the SWNT [39]. Tripathy et al. suggested that the dependence of conductance on the crossing angle between nanotubes in junctions is due to the overlap of the π orbitals [19], which is also a possible explanation for the observation shown here. Here, it is speculated that when both SWNTs are rotationally aligned (at 0°, shown in (a) of Fig. 4.4), the π orbitals on the junction interface overlap; in addition to the intratube π orbital interaction, this improves the junction conductance. As the rotational misalignment increases,

the overlap region shrinks, and in turn reduces the junction conductance.

4.2 Potassium Doped Junction

The first of the two doped junctions examined was the K doped junction. Two doping configurations were selected – the external doping and the interstitial doping configurations for the junctions. The motivation for studying the external doping configuration was the positive results shown in the previous chapter on SWNT conductors. Study of the interstitial doping configuration was inspired by the work on polyiodide doped CNT junctions [10]. The two doping configurations for the K doped junctions are shown in Fig. 4.7.

In order to assign packing arrangements for the different doping configurations, another set of equations was defined to describe the computational unit cell dimensions required to accommodate the change in packing arrangement caused by the presence of dopants. Similar to the process used for the undoped junctions, the equilibrium nanotube separation distance ($l^*_{SWNT-SWNT}$) was obtained after structural relaxation. In addition, the dopant standoff ($l^*_{dopant-SWNT}$) and dopant separation distance ($l^*_{dopant-dopant}$) were obtained, respectively, for the externally doped and interstitially doped junctions.

Next, alternate end segments were removed (at equal lengths, along with the electrode dopants) depending on the overlap distance desired, for transport calculations. The doped SWNT junction was packed into a compu-

tational unit cell of dimensions $x_{junc} \times y_{junc} \times z_{junc}$, defined as

$$x_{junc} = \begin{cases} l^*_{SWNT-SWNT} + d_{SWNT} & \text{for the external doping configuration} \\ 2l^*_{dopant-dopant} & \text{for the interstitial doping configuration} \end{cases} \tag{4.4}$$

$$y_{junc} = \begin{cases} 4l^*_{dopant-SWNT} + \\ l^*_{SWNT-SWNT} + 2d_{SWNT} & \text{for the external doping configuration} \\ 2l^*_{SWNT-SWNT} + 2d_{SWNT} & \text{for the interstitial doping configuration} \end{cases} \tag{4.5}$$

$$z_{junc} = \text{length of the model} \tag{4.6}$$

where d_{SWNT} is the diameter of the SWNT conductor. Due to the size of the K atom, which spans the length of one unit cell in the (5,5) SWNT, the K doped junctions were doped at one atom per two unit cells. This led to the total number of unit cells for each K doped SWNT conductor in the junctions to be a multiple of two. In the K doped junctions, the SWNT conductors were 16 unit cells long (before removal of the ends). Figures 4.2 (right) and 4.3 show the computational unit cells for the different doping configurations.

For the external K doping configuration, the nanotube separation distance ($l^*_{SWNT-SWNT}$) was 3.46 Å, and the dopant standoff ($l^*_{dopant-SWNT}$) was 2.62 Å. For the interstitial K doping configuration, the nanotube separation distance ($l^*_{SWNT-SWNT}$) was 3.41 Å, and the dopant separation distance ($l^*_{dopant-dopant}$) was 6.42 Å. The dimensions for the computational unit cells used are listed in Table 4.1.

Both doping configurations improved the conductance of the (5,5) junctions, as shown in Fig. 4.9. The highest conductivity K doped junction had

conductance of $1.02G_0$. It was obtained with the interstitial doping configuration at an overlap distance of seven unit cells, with the nanotube packing rule (in the x_{junc} direction) derived from the rule for interstitially doped models (shown on the right of Fig. 4.2 yielding $x_{junc} = 12.84$ Å). The external doping configuration performed similarly to the interstitial doping configuration; they both improved the conductance by a factor of 2-2.5 at all overlap distances.

The effect of packing arrangement was further investigated, done by using the packing rule (in the x_{junc} direction) for undoped junction models (shown on the left of Fig. 4.2) to reduce the computational unit cell size. On the right of Fig. 4.9 the effect of the packing arrangement on the conductance can be seen. The conductance of the K interstitially-doped junction decreased when the nanotube packing (in x_{junc}) was reduced from 12.84 Å (based on Eqn. (4.4), the interstitial doping x_{junc} rule) to 10.47 Å (based on Eqn. (4.1), the undoped x_{junc} rule). Unlike the undoped junctions, the reduction in packing density reduced the conductance of the interstitially doped K junctions.

4.3 Tetrabromoaurate Doped Junction

The second of the two doped junctions examined was the $AuBr_4$ doped junction. Like the K doped junctions, the external doping and interstitial doping configuration were modeled for the $AuBr_4$ doped junction. The ends removal process was identical to that used for the K doped junction, as described in the previous subsection.

Using the values obtained after structural relaxation to determin the

nanotube separation distance ($l^*_{SWNT-SWNT}$), dopant standoff ($l^*_{dopant-SWNT}$), and dopant separation distance ($l^*_{dopant-dopant}$), the $AuBr_4$ doped junctions were packed based on the rules set for the doped junctions, listed in Eqns. (4.4), (4.5), and (4.6). Due to the size of the $AuBr_4$ fragment, which spans the length of three unit cells, in the (5,5) SWNT, the $AuBr_4$ doped SWNT were doped at one fragment per three unit cells. This led to the total number of unit cells of each $AuBr_4$ doped SWNT conductor in the junction to be a multiple of three. In the $AuBr_4$ doped junctions, the SWNTs were 15 unit cells long before the removal of the ends. Figures 4.2 (right) and 4.3 show the computational unit cells for the different doping configurations.

For the external $AuBr_4$ doping configuration, the nanotube separation distance ($l^*_{SWNT-SWNT}$) was 3.39 Å, and the dopant standoff ($l^*_{dopant-SWNT}$) was 3.36 Å. For the interstitial $AuBr_4$ doping configuration, the nanotube separation distance ($l^*_{SWNT-SWNT}$) was 3.79 Å, and the dopant separation distance ($l^*_{dopant-dopant}$) was 11.43 Å. The dimensions for the computational unit cells used are listed in Table 4.1.

Depending on the type of dopant configuration, the $AuBr_4$ fragment had a mixed effect on the (5,5) junction, as shown in Fig. 4.9. The external doping configuration had an adverse effect on the junction conductance, which was reduced to $\leq 0.41G_0$ across the different overlap distances. The interstitial doping configuration however, had a large positive effect on the junction conductance. At an overlap distance of five unit cells, the conductance exceeded the benchmark value for an undoped (5,5) SWNT at $2.04G_0$. The conduc-

tance for the interstitially doped $AuBr_4$ junction was also independent of the junction overlap; for all overlap distances the conductance stayed in the range of $1.8G_0$.

4.4 Discussion

The junction conductance of the (5,5) SWNT is sensitive to the following variables:

- Nanotube separation distance, $l_{SWNT-SWNT}$. The junction conductance was highest between $l_{SWNT-SWNT} = 2.5$ to 3.0 Å, much higher than the junction conductance at $l^*_{SWNT-SWNT} = 3.36$ Å. However, the system was more energetically favorable at $l^*_{SWNT-SWNT}$ than at any of the other $l_{SWNT-SWNT}$. External constraining forces (through physical or chemical means, in addition to the densification shown in [6, 7]) could perhaps reduce the nanotube separation distance, such that the SWNT junctions' energetic state is not minimized.

- Junction overlap distance. An nonmonotonic behavior of the junction conductance was observed, as the overlap distance was increased. Such behavior is common in graphene and SWNT junctions [23, 38], and although longer SWNT junctions (i.e. longer overlap distances) can capture the behavior over larger ranges, computational costs are a concern for models of such size.

- Rotational misalignment. The rotational misalignment of the junctions

drastically reduced the conductance, and was likely due to the reduction in the π bond overlap as the misalignment increases. It is perhaps possible that doping can reduce the conductance loss induced by rotational alignment, but this has not been investigated in this work.

- Packing arrangement. For the undoped SWNT junctions, the conductance raised sharply when the packing arrangement was reduced from the isolated relaxation case (with $l^*_{SWNT-SWNT}$ = 3.36 Å) to $l_{SWNT-SWNT}$ = 2.5 - 3.0 Å, before dropping off as $l_{SWNT-SWNT} < 2.5$ Å. It appears that the radial densification as performed by experimental researchers in [7] has a positive effect on the undoped junction conductance. In the interstitially K doped junctions however, the conductance decreased when x_{junc} went from 12.84 Å to 10.47 Å. More data points on the packing of K doped junctions will be needed in order to obtain a verdict on the ideal packing size. As it stands now, the reduction in packing of the interstitial K doped junction from $x_{junc} = 2l^*_{dopant-dopant}$= 12.84 Å is detrimental to conductance.

- K and $AuBr_4$ doping. The K atom had a positive effect on the junction, in both the external and interstitial doping configuration. Both doping configurations have conductance that are quite similar across different overlap distances. As for the $AuBr_4$ doped junctions, only the interstitial doping configuration improved the junction conductance, while the external doping configuration reduced the conductance, as compared to the

undoped junction. According to Saito, the most effective type of dopant in inducing charge transfer in CNTs would be a highly electropositive element, like alkali metals [40]. This could explain why the conductance for the K doped junctions were less dependent on the dopant configuration, as compared to the $AuBr_4$ doped junctions. The conductance for the K doped junctions were quite consistent across the different doping configurations, whereas the conductance for the $AuBr_4$ doped junctions varied significantly. For the $AuBr_4$ doped junction, the proximity of the dopant to the CNT interface seems to be important; the positioning of the $AuBr_4$ fragments closer to the interface seems to raise the junction conductance. As for the most likely doping configuration for both types of dopants, a molecular dynamics (MD) simulation may be able to provide a suggestion on that. However, for a DFT based model, the computational costs required are likely to be unacceptable. Future work could involve investigations using MD simulation.

Table 4.1: Computational unit cell dimensions of junction models.

Dopant	Dopant Configuration	x_{junc} (Å)	y_{junc} (Å)	z_{junc} (Å)
Undoped	N/A	10.33	20.52	36.92
K	External	10.38	27.65	39.38
	Interstitial	12.84	20.39	39.38
$AuBr_4$	External	10.31	30.44	36.92
	Interstitial	22.86	21.37	36.92

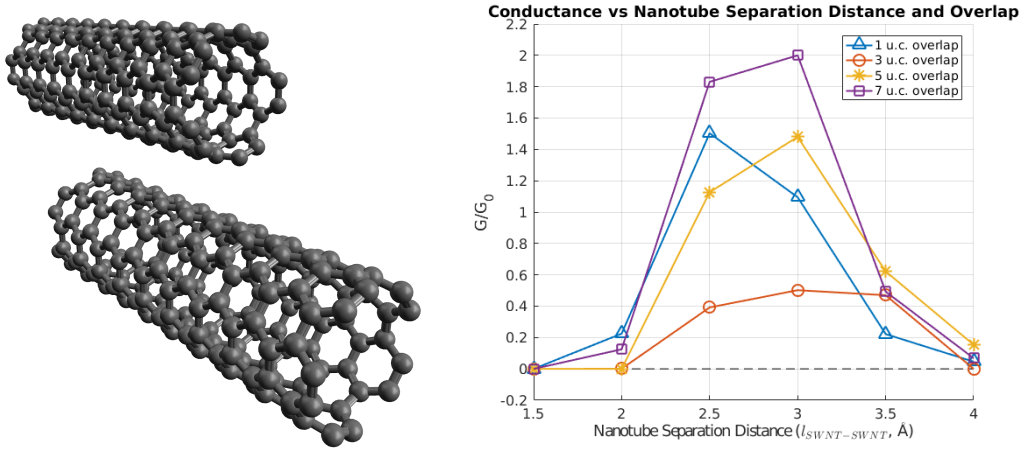

Figure 4.1: Undoped junction with a five unit cell overlap (left), and conductance of the undoped (5,5) junctions as a function of varying overlap distance and nanotube separation distance ($l_{SWNT-SWNT}$) for 0° rotation (right).

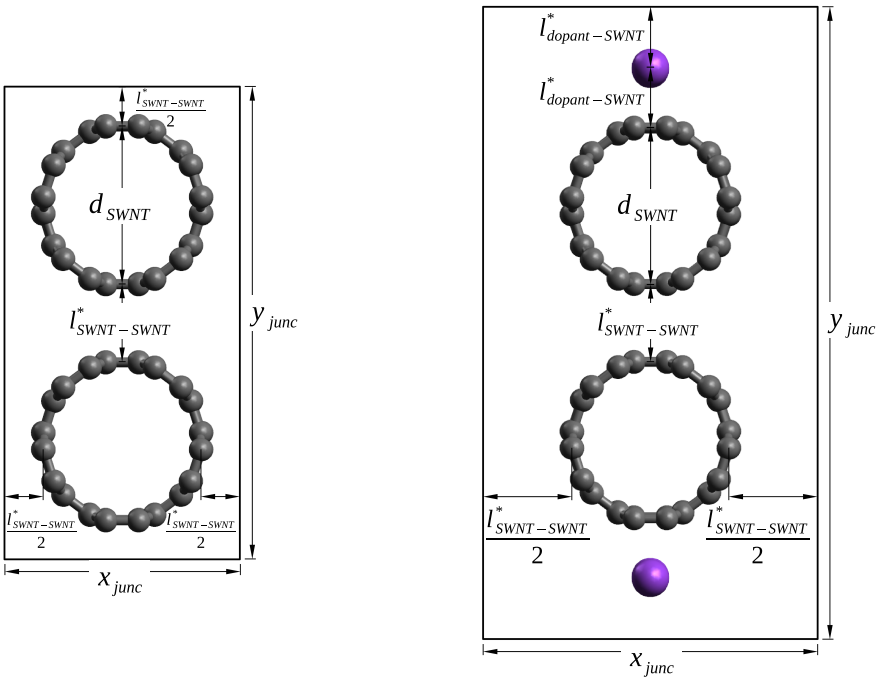

Figure 4.2: Axial (projected) view of a computational unit cell for an undoped (left) and externally doped (right) junction (note that z_{junc} is the model length in the axial direction).

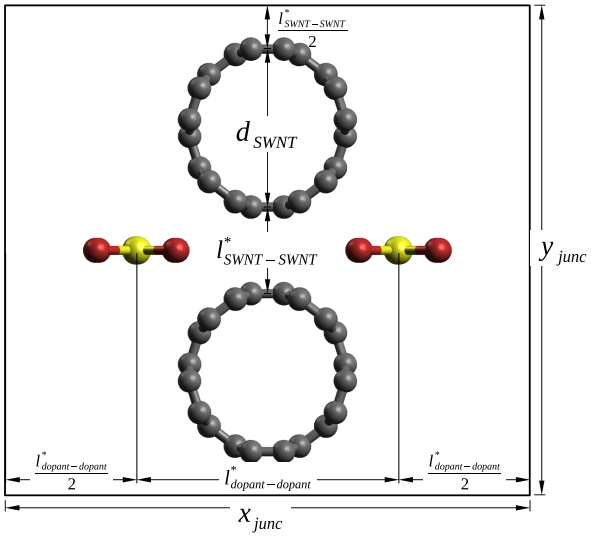

Figure 4.3: Axial (projected) view of a computational unit cell for an interstitially doped junction (note that z_{junc} is the model length in the axial direction).

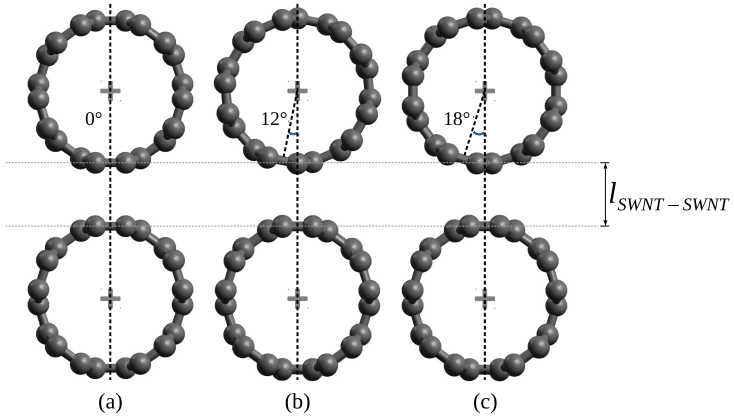

Figure 4.4: Axial (projected) view of three SWNT junctions for three different rotational alignments (0°, 12° and 18°).

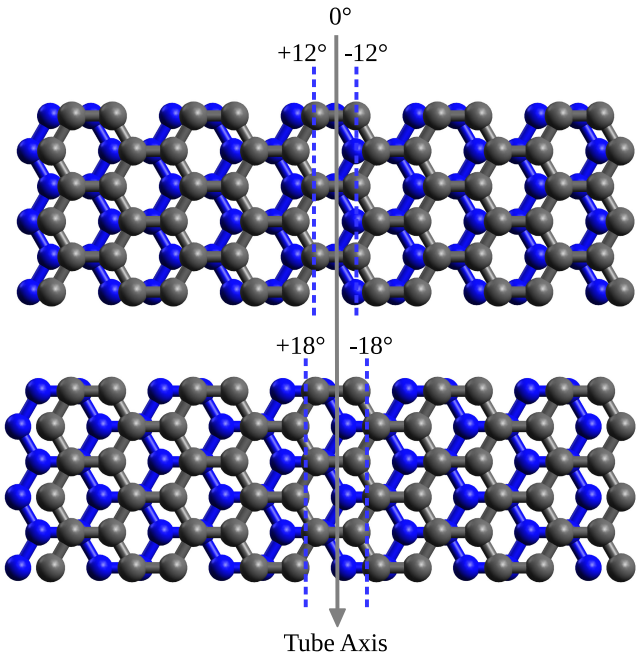

Figure 4.5: Unrolled SWNTs for the rotationally misaligned junctions at 12° (top) and 18° (bottom); the grey (lighter) atoms represent the lower SWNT (in Fig. 4.4), and the blue (darker) atoms represent the upper SWNT (in Fig. 4.4).

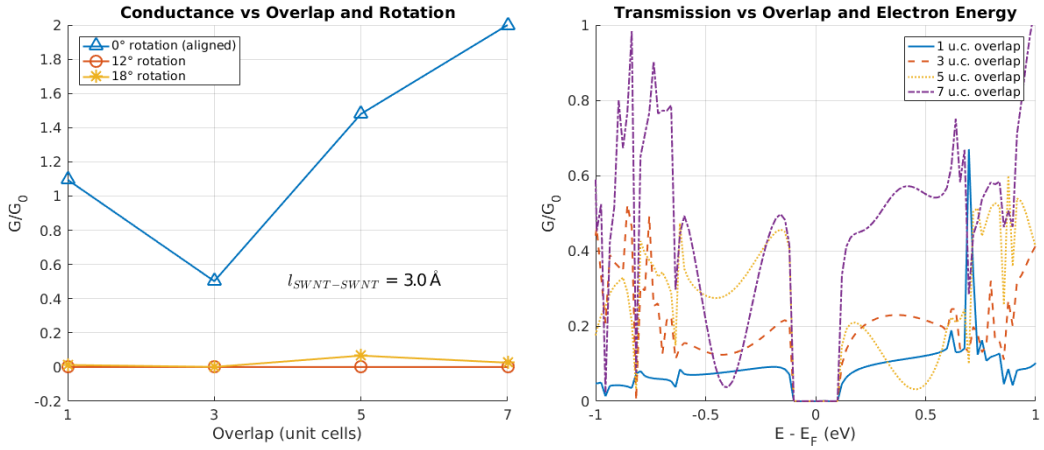

Figure 4.6: On the left, conductance of the 12° and 18° rotationally misaligned junctions as a function of overlap, at a nanotube separation distance ($l_{SWNT-SWNT}$) of 3.0 Å; on the right, conductance of the 12° rotationally misaligned junction as a function of overlap and electron energy. In this work, the transmission data from the transport calculations was obtained through the sampling of 201 points between -2 eV to +2 eV.

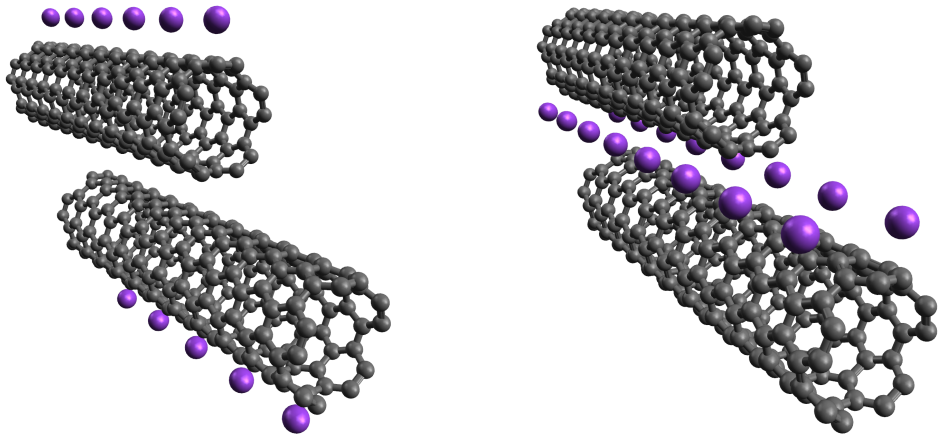

Figure 4.7: K doped junctions: externally doped (left) and interstitially doped (right).

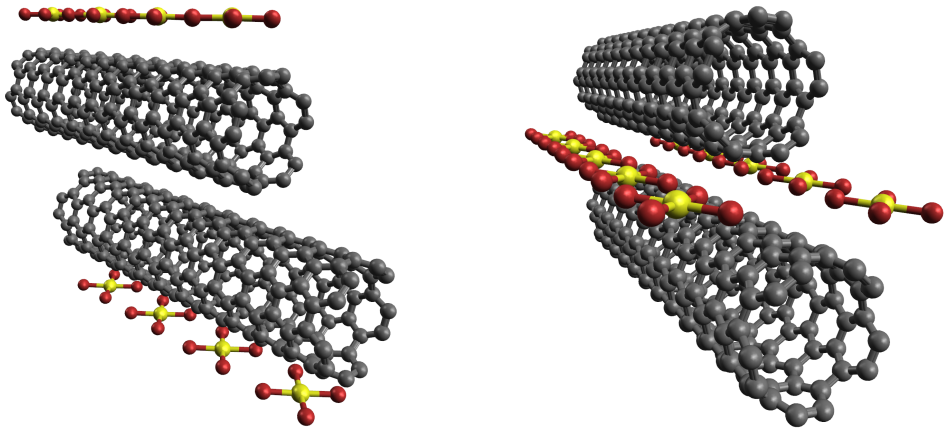

Figure 4.8: $AuBr_4$ doped junctions: externally doped (left) and interstitially doped (right).

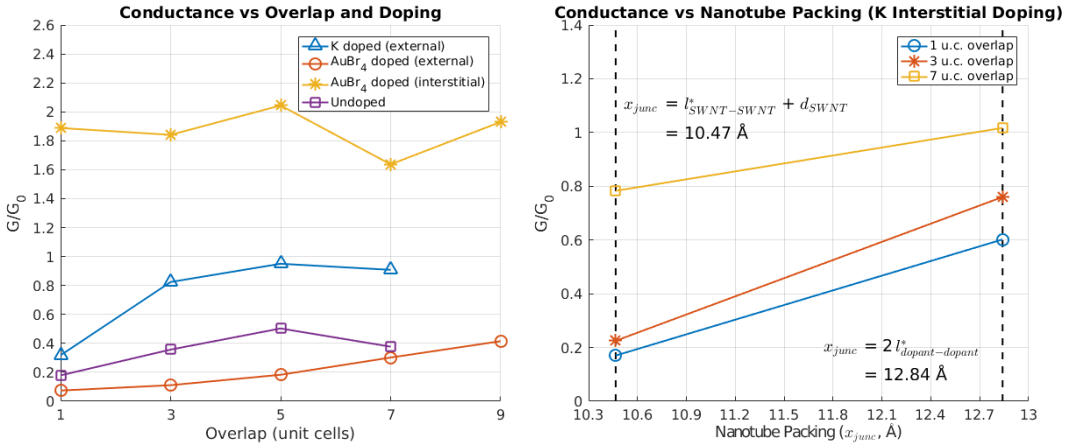

Figure 4.9: On the left, effects of overlap and dopant configuration on conductance; on the right, effects of overlap and nanotube packing on conductance.

Chapter 5

Nanowire Model

In this chapter, a method to describe the macro-scale performance of CNTs is presented. A nanowire model is proposed to compute specific conductivity, which is used as a performance metric M. The performance of the nanowires is evaluated through a comparison of specific conductivity to the specific conductivity of copper.

The metric M for the nanowire is based on previous work [10], given by the following equation that describes the specific conductivity the specific conductivity of a non-continuum material:

$$\frac{1}{M} = \frac{\rho}{\sigma} = \hat{m}_{eff}\frac{R_{eff}}{L_{MFP}},\ R_{eff} = \frac{1}{\min(G_c, G_j)}, \tag{5.1}$$

where ρ and σ are the mass density and conductivity of a continuum material respectively, $\hat{m}_{eff}$ is the effective mass per unit length of the nanowire, L_{MFP} is the mean free path length in CNTs, R_{eff} is the effective resistance of the nanowire, and G_c (or G_j) is the conductance of the conductor (or junction). The 'min' function ensures that the nanowire model can only allow electronic transmission at the lower conductance (between the conductor and junction), since that would be the limiting factor for electronic transport. The effective

mass per unit length is defined as

$$\hat{m}_{eff} = (1-\alpha)\hat{m}_c + \alpha\hat{m}_j,\ \hat{m}_c = \frac{m_c}{L_c},\ \hat{m}_j = \frac{m_j}{L_j},\ \text{and}\ \alpha = \frac{L_j}{L_{MFP}}, \qquad (5.2)$$

where m_c (or m_j) is the mass of a conductor (or junction) with the length L_c (or L_j). Here, α is defined as the fractional overlap of the nanowire.

Table 5.1 shows the fractional overlap, mass per unit length, packing density, and conductance values for the junctions. The highest and lowest conductance results for the junction models (with regard to the fractional overlap, mass per unit length, and packing density) were considered for the nanowire model. The packing density for the junctions is simply the number of SWNT conductors in the junction divided by the axial (projected) area of the computational unit cell, i.e., $2/(x_{junc}y_{junc})$.

The nanowire performance metric M in its functional form is expressed as:

$$M = f(m_c, m_j, L_c, L_j, G_c, G_j) \qquad (5.3)$$

where the values for the variables were obtained from the models presented in Sections 3 and 4. Since two different doping concentrations were studied for the conductor models, and two doping configurations were studied for the junction models, four combinations of conductor and junction models were analyzed to create the nanowire model. The properties of the models are shown in Table 5.2.

The results of the nanowire model were compared to a continuum conductor made of copper, designated as the reference metric, M_{ref}. Since the

reference metric was obtained from a continuum model, the specific conductivity formula (shown as the inverse in Eqn. (5.1)) only requires the conductivity (σ) and the mass density (ρ), which yields $M_{ref} = 6671.30$ Sm kg^{-1} [41]. A mean free path of $L_{MFP} = 500$ nm was chosen for the nanowire model, based of a study on metallic SWNTs [42]. The effects of the dopants on the mean free path of CNTs are not clear, and there is no agreement in mean free path even for undoped CNTs. The type of CNTs tested in the experiments by Mann et al. [42] is similar to that in the present research, which was why the mean free path value of 500 nm (from the results in [42]) was assumed.

Figure 5.1 shows a comparison of specific conductivity predicted by the nanowire model versus copper. The metrics for different combinations had different ranges. Notably, the K doped nanowire showed a wider variation (shown on the left) than the $AuBr_4$ doped nanowire (shown on the right). In fact, the $AuBr_4$ doped nanowire was extremely sensitive to the junction doping configuration. Quantitatively, the specific conductivity factor over copper for the K doped nanowire ranged from 0.524 to 3.357, while the factor for the $AuBr_4$ doped nanowire ranged from 0.154 to 4.164. The experimental specific conductivity factor for the $KAuBr_4$ doped CNT in [7], shown in black dashed lines in Fig. 5.1, was 0.73 (73% of the specific conductivity of copper) at 4842.86 Sm^2 kg^{-1}, and is within the computed ranges for the K doped and $AuBr_4$ doped nanowires.

It is noted that the nanowire model presented in this work is expected to outperform the experimental data obtained from [7]. In that work, the $KAuBr_4$

doped CNT consisted of nanotubes that were SWNTs and MWNTs, and possibly included a mixture of both metallic and semiconducting nanotubes. Hence, the observed difference of the experimental specific conductivity, as compared to the nanowire models, is reasonable. Furthermore, the experimental doping configuration is undetermined for the $KAuBr_4$ doped CNT; the dopant could either adsorb to the CNTs in its disassociated form (as K atoms and $AuBr_4$ fragments) or as a complete $KAuBr_4$ molecule, or both. These factors could all contribute to the discrepancy between the nanowire performance and the experimental data in Fig. 5.1. Moreover, the fractional overlap α may vary form junction to junction. Hence the nanowire model is a 'high performance model' and it estimates a higher specific conductivity than the experimental reference indicates. Percolation modeling might be able to provide a closer estimate, but it is beyond the scope of this thesis, which is limited to quantum analysis.

The tabulated nanowire models in Table 5.2 represent high performance configurations for the different types of disassociated dopants, for strictly metallic SWNT conductors and junctions.

Table 5.1: Fractional overlap, mass per unit length, packing density and conductance for the doped junctions.

Dopant	Dopant Configuration	Fractional Overlap α ($\times 10^{-3}$)	Mass per Unit Length $\hat{m}_j$ (amu Å^{-1})	Packing Density ($\times 10^{-3}$ Å^{-2})	Conductance G_j/G_0
K	External	0.246	390.7	6.968	0.318
		1.230	253.4	6.968	0.824
		2.215	231.1	6.968	0.950
		3.199	227.4	6.968	0.908
	Interstitial	0.246	391.1	7.639	0.602
		1.230	260.0	7.639	0.760
		3.197	230.0	7.639	1.017
		0.246	391.1	9.368	0.170
		1.230	260.0	9.368	0.225
		3.197	230.0	9.368	0.783
$AuBr_4$	External	0.246	681.5	6.373	0.074
		1.229	402.7	6.373	0.111
		2.213	324.9	6.373	0.183
		3.197	339.7	6.373	0.302
		4.182	355.0	6.373	0.415
	Interstitial	0.246	971.4	4.094	1.888
		1.230	402.4	4.094	1.841
		2.214	339.2	4.094	2.044
		3.199	364.1	4.094	1.637
		4.183	355.0	4.094	1.930

Table 5.2: Combinations of conductors and junctions considered in the nanowire model calculation.

Dopant	Conductor Dopant Concentration (dopant/u.c.)	Junction Doping Configuration
K	0.50	External
	0.50	Interstitial
	1.00	External
	1.00	Interstitial
$AuBr_4$	0.33	External
	0.33	Interstitial
	0.67	External
	0.67	Interstitial

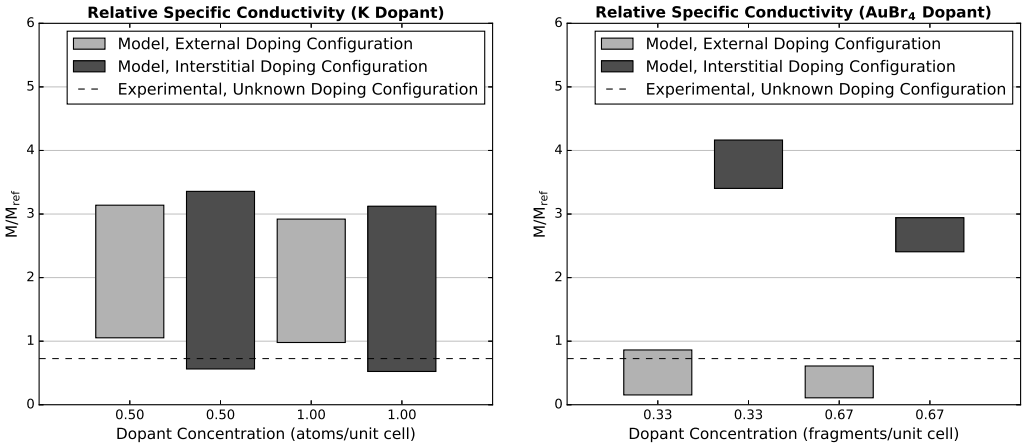

Figure 5.1: The relative specific conductivity of the K doped nanowire (left) and $AuBr_4$ doped nanowire (right), with the dashed line indicating the specific conductivity of the $KAuBr_4$-doped CNT (of which the doping origin is undetermined) in [7] as compared to M_{ref}; the experimental reference is meant to show the plausibility of the presented nanowire model, not as a direct comparison.

Chapter 6

Conclusion

The principal findings of this research on $KAuBr_4$, K, and $AuBr_4$ doped models are presented in this chapter. Motivated by previous works, where experimental literature showed that the $KAuBr_4$ doped CNTs had a very high conductivity [6, 7], this thesis studied computational models of the $KAuBr_4$ doped CNTs. (Similarly, experimental literature showed that iodine doped CNTs had a very high specific conductivity [3], and a previous work [10] studied computational models of the iodine doped CNTs.)

From the SWNT conductors models, it was found that:

- $KAuBr_4$ improved the conductance of the (5,5) SWNT conductor, but not the (8,0) SWNT conductor. The conductance of the doped (5,5) conductor was raised to $4G_0$ at 0.67 dopant molecules per unit cell, while the conductance of the doped (8,0) conductor remained at zero. Despite the improvement to the conductance, the $KAuBr_4$ doped (5,5) conductor had a decrease in the specific conductance, lower than the benchmark of an undoped (5,5) conductor (the specific conductance was zero for the (8,0) conductor). This was due to the high dopant mass fraction introduced by the $KAuBr_4$ molecule, as high as 60% for the

(8,0) conductor, and as high as 61% for the (5,5) conductor. Since bulk CNT's consist of a mixture of metallic and semiconducting nanotubes [37], it is possible to have an increase in overall conductivity if only the metallic SWNT has an improvement in conductance; thus the results are consistent qualitatively with experiment [6, 7].

- K improved both the conductance (5,5) and the (8,0) SWNT conductors drastically. The conductance increased to as high as $2.5G_0$ for the (8,0) conductor and $3.8G_0$ for the (5,5) conductor. The specific conductance was also increased for both conductors, past the benchmark value for an undoped (5,5) conductor. This was due to the low dopant mass fraction introduced by the K atom, only 9% for the (8,0) conductor, and 14% for the (5,5) conductor. This improvement in conductance is consistent with computational and experimental literature [8, 13].

- $AuBr_4$ improved both the (5,5) and the (8,0) SWNT conductors drastically. The conductance increased to as high as $1.9G_0$ for the (8,0) conductor and $4G_0$ for the (5,5) conductor. However, due to the large mass of the $AuBr_4$ fragments, specific conductance for both the (8,0) and the (5,5) conductors was lower than the benchmark for an undoped (5,5) SWNT conductor. The dopant mass fraction for the $AuBr_4$ fragment for the (8,0) conductor was as high as 57%, and for the (5,5) conductor it was as high as 59%. The increase in conductance of the $AuBr_4$ doped SWNT conductor is consistent with related work on $AuCl_4$, which ex-

hibited improvement to its conductance of SWNT [16]. (Related work on $AuBr_4$ doped CNTs, computational or experimental, was not found.)

As for the (5,5) SWNT junctions, it was found that:

- The nanotube separation distance of $l^*_{SWNT-SWNT} = 3.36$ Å was obtained from relaxing two isolated and undoped SWNT conductors, but with a slight decrease of nanotube separation distance (to $l_{SWNT-SWNT}$ = 2.5 to 3.0 Å) (increase in the packing density) the junction conductance increased sharply.

- The junction overlap distance had a nonmonotonic effect on the junction conductance, which was expected from previous work [23, 38]. Fig. 4.1 shows that at constant separation distances, the variation of the conductance with overlap was not monotonic.

- The rotational configuration had an important effect on the junction conductance. The decrease in conductance due to rotational misalignment between the SWNT conductors in the junction can be described as the reduction in π orbital overlap between the conductors; similar behavior was found in [19].

- The packing arrangement affected the junction conductance. As seen in the undoped SWNT junction, the conductance can be increased by a slight reduction in packing density, which indicated that densificaton [7] may be beneficial. However, there may be a limit to how much packing

can help: for the interstitially K doped junction, the reduction in packing reduced the conductance.

- K had a positive effect on the SWNT junction conductance, and was not quite as sensitive to different doping configurations. On the other hand, the interstitially doped $AuBr_4$ junction was significantly better than the externally doped $AuBr_4$ junction in increasing junction conductance. As pointed out by Saito, alkali metals are the leading candidates in altering nanotube electronic states [40], and this supports the argument that the K atom affects the SWNT junctions' electronic state more than the $AuBr_4$ fragments: the K atom as an alkali metal is extremely reactive, and has a higher tendency to alter the electronic state of the SWNT junctions as compared to the $AuBr_4$ fragment, which was heavily dependent on dopant configuration for high conductance.

The nanowire model provided a metric to compare the findings with the experimentals of [7], as well as to bulk copper. The experimental specific conductivity of the $KAuBr_4$ doped CNT fell within the range of the nanowire model values. As expected, the high performance configuration nanowire models had a specific conductivity higher than the experimental value, since many factors such as the doping configuration and the mixture of nanotubes could lower the experimental value. Note that it is possible to experimentally produce doped CNTs with specific conductivity much higher than that of copper: Zhao et al. showed that with iodine doping, the specific conductivity of nanotube cables can surpassed copper's by a factor of three [3] (although the

nanotubes in question are double walled, which are metallic even if both the inner and outer nanotubes are semiconducting [43]).

The results in this work show the potential of SWNT wires doped with $KAuBr_4$, K, and $AuBr_4$ for conductive wires (especially K in mass specific applications) and can assist future experimental efforts in the investigation of doped-SWNT conductive wires. As a follow up on the work in this thesis, the investigation of dispersion corrected models, as well as the possibility of utilizing finite temperature methods to analyze the doped models, may be considered. Such work may further improve the understanding of $KAuBr_4$ doped CNTs.

Appendix

Appendix A

Ion Doped Conductor Models

The doping solution used in works that produced the $KAuBr_4$ doped CNT was a $KAuBr_4$ aqeuous solution [6, 7], which raised the possibility of K^+ and $AuBr_4^-$ ions as doping agents in the solution. Hence, the two ion dopants were considered as candidates for the doped models.

Since the mass of an electron is much smaller than the atomic mass of the element, the atomic masses of the dopants remain the same, shown in Table 3.2. Similar to the SWNT models with charge neutral dopants, two dopant concentrations were tested for the ions. Transport calculations for the ion doped conductors were done by initializing the models as electron-deficient or -surplus, respectively, for the K^+ and the $AuBr_4^-$ cases.

A.1 Potassium Ion

First, the K^+ doped SWNT conductor was studied. The K^+ ion spans the length of one unit cell in both the (8,0) and (5,5) SWNTs. Hence, the dopant concentrations are 0.50 and 1.00 ion per unit cell for both the (8,0) and (5,5) SWNT conductors. The distances of K^+ dopants from the SWNT and the doped mass per unit length is listed in Table A.1.

The K^+ ion had no effect on the conductance, for either the (8,0) or the (5,5) conductors. Table A.1 shows the performance of the K^+ doping on both types of conductors. With no increase in conductance, the specific conductance of the K^+ doped SWNT conductor remained at zero for the (8,0) conductor, and decreased for the (5,5) conductor.

A.2 Tetrabromoaurate Ion

Next, the $AuBr_4^-$ ion was studied, the other part of the $KAuBr_4$ molecule. The $AuBr_4^-$ ion spans the length of two unit cells in the (8,0) SWNT, and three unit cells in the (5,5) SWNT. Hence, the $AuBr_4^-$ dopant concentrations tested are 0.50 and 1.00 ion per unit cell for the (8,0) SWNT. Correspondingly, the dopant concentrations are 0.33 and 0.67 ion per unit cell for the (5,5) SWNT. The distances of $AuBr_4^-$ dopants from the SWNT and the doped mass per unit length is listed in Table A.1.

The $AuBr_4^-$ ion had no effect on the conductance, for either the (8,0) or the (5,5) SWNT conductor. Table A.1 shows the performance of the $AuBr_4^-$ doping on both conductors. With no improvement to the conductance, the specific conductance of the $AuBr_4^-$ doped SWNT conductor remained at zero for the (8,0) conductor, and decreased for the (5,5) conductor.

Table A.1: Dopant standoff (from SWNT surface), mass per unit length, and conductance for the doped conductors. The specific conductance can be obtained from taking the ratio of the conductance (column 6) to the mass per unit length (column 5).

Dopant	SWNT Chirality	Concentration (number/ u.c.)	Dopant Standoff $l_{dopant-SWNT}$ (Å)	Mass per Unit Length $\hat{m}_c$ (amu Å^{-1})	Conductance G_c/G_0
K^+	(8,0)	0.50	2.503	94.8	0.000
		1.00	2.440	99.3	0.000
	(5,5)	0.50	2.546	105.5	1.993
		1.00	2.936	113.5	1.994
$AuBr_4^-$	(8,0)	0.50	3.163 (Au)	150.8	0.000
		1.00	3.296 (Au)	211.3	0.000
	(5,5)	0.33	3.377 (Au)	167.6	1.991
		0.67	3.506 (Au)	237.5	1.996

Bibliography

[1] Iijima, S., 1991, "Helical Microtubules of Graphitic Carbon," Nature, **354**, pp. 56-58.

[2] Puchades, I., Lawlor, C. C., Schauerman, C. M., Bucossi, A. R., Rossi, J. E., Cox, N. D., and Landi, B. J., 2015, "Mechanism of Chemical Doping in Electronic-Type-Separated Single Wall Carbon Nanotubes Towards High Electrical Conductivity," Journal of Materials Chemistry C, **3**(39), p. 10256.

[3] Zhao, Y., Wei, J., Vajtai, R., Ajayan, P. M., and Barrera, E. V., 2011, "Iodine Doped Carbon Nanotube Cables Exceeding Specific Electrical Conductivity of Metals," Scientific Reports, **1**, p. 83.

[4] Lee, P., Ham, J., Lee, J., Hong, S., Han, S., Suh, Y. D., Lee, S. E., Yeo, J., Lee, S. S., Lee, D., and Ko, S. H., 2014, "Highly Stretchable or Transparent Conductor Fabrication by a Hierarchical Multiscale Hybrid Nanocomposite," Advanced Functional Materials, **24**(36), pp. 5671-5678.

[5] Janas, D., Milowska, K. Z., Bristowe, P. D., and Koziol, K. K. K., 2017, "Improving the Electrical Properties of Carbon Nanotubes with Interhalogen Compounds," Nanoscale, **9**(9), pp. 3212-3221.

[6] Alvarenga, J., Jarosz, P. R., Schauerman, C. M., Moses, B. T., Landi, B. J., Cress, C. D., and Raffaelle, R. P., 2010, "High Conductivity Carbon Nanotube Wires from Radial Densification and Ionic Doping," Applied Physics Letters, **97**(18), p. 182106.

[7] Cress, C. D., Ganter, M. J., Schauerman, C. M., Soule, K., Rossi, J. E., Lawlor, C. C., Puchades, I., Ubnoske, S. M., Bucossi, A. R., and Landi, B. J., 2017, "Carbon Nanotube Wires with Continuous Current Rating Exceeding 20 Amperes," Journal of Applied Physics, **122**(2), p. 025101.

[8] Lee, R. S., Kim, H. J., Fischer, J. E., Thess, A., and Smalley, R. E., 1997, "Conductivity Enhancement in Single-Walled Carbon Nanotube Bundles Doped with K and Br," Nature, **388**(6639), pp. 255-257.

[9] Kim, K. K., Bae, J. J., Park, H. K., Kim, S. M., Geng, H., Park, K. A., Shin, H., Yoon, S., Benayad, A., Choi, J., and Lee, Y. H., 2008, "Fermi Level Engineering of Single-Walled Carbon Nanotubes by AuCl3 Doping," Journal of the American Chemical Society **130**(38), pp. 12757-12761.

[10] Li, Y., and Fahrenthold, E., 2018, "Ab Initio Study of Iodine-Doped Carbon Nanotube Conductors," Journal of Engineering Materials and Technology, **140**(2), p. 021008.

[11] Salzer, A., 1999, "Nomenclature of Organometallic Compounds of the Transition Elements (IUPAC Recommendations 1999)," Pure and Applied Chemistry, **71**(8), pp. 1557-1585.

[12] Li, X., Liu, J., Kong, F., Liu, X., Xu, J., and Chen, H., 2012, "Potassium-Doped Graphene for Simultaneous Determination of Nitrite and Sulfite in Polluted Water," Electrochemistry Communications, **20**, pp. 109-112.

[13] Miyake, T., and Saito, S., 2002, "Electronic Structure of Potassium-Doped Carbon Nanotubes," Phyiscal Review B, **65**(16), p. 165419.

[14] Kim, S. M., Kim, K. K., Jo, Y. W., Park, M. H., Chae, S. J., Duong, D. L., Yang, C. W., Kong, J., and Lee, Y. H., 2011, "Role of Anions in the $AuCl_3$-Doping of Carbon Nanotubes," ACS Nano, **5**(2), pp. 1236-1242.

[15] Murat, A., Rungger, I., Jin, C., Sanvito, S., and Schwingenchlögl, U., 2014, "Origin of the p-Type Character of $AuCl_3$ Functionalized Carbon Nanotubes," Journal of Physical Chemistry C, **118**(6), pp. 3319-3323.

[16] Ketolainen, T., Havu, V., and Puska, M. J., 2017, "Conductivity of $AuCl_4$-Functionalizd Carbon Nanotube Networks," The Journal of Physical Chemistry C, **121**(8), pp. 4627-4634.

[17] Li, E., and Marzari, N., 2011, "Improving the Electrical Conductivity of Carbon Nanotube Networks: A First-Principles Study," ACS Nano, **5**(12), pp. 9726-9736.

[18] Saito, S., 1999, "Electronic Properties of Potassium-Doped Carbon Nanotube Lattice, Amorphous and Nanostructured Carbon, Sullivan, J.P., Robertson, J., Zhou, O., Allen, T. B., and Coll, B. F., 1^{st} ed., Vol. **593**

MRS Symposium Proceedings, Materials Research Society, Pennsylvania, USA, pp. 161-166.

[19] Tripathy, S., and Bhattacharyya, T. K., 2016, "Role of Inter-Tube Coupling and Quantum Interference on Electrical Transport in Carbon Nanotube Junctions," Physica E, **83**, pp. 314-321.

[20] Li, T. S., Huang, Y. C., Lin, M. F., and Chang, S. C., 2010, "Conductance of Bilyaer Graphene Nanoribbons with Different Widths," Philosophical Magazine, **90**(23), pp. 3177-3187.

[21] Wang, J., Lin, Z., and Chan, K. S., 2014, "The Effect of Interlayer Coupling on Electron Transport in Graphene Nanoribbons: A Potential Method for Nanoposition Sensing," Journal of Physics: Condensed Matter, **26**(13), p. 135301.

[22] Benameur, M. M., Gargiulo, F., Manzeli, S., Autès, G., Tosun, M., Yazyev, O. V., and Kis, A., 2015, "Electromechanical Oscillations in Bilayer Graphene," Nature Communications, **6**, p. 8582.

[23] González, J. W., Santos, H., Pacheco, M., Chico, L., and Brey, L., 2010, "Electronic Transport through Bilayer Graphene Flakes," Physical Review B, **81**(19), p. 195406.

[24] Srivastava, S., Kino, H., and Joachim, C., 2016, "Contact Conductance of a Graphene Nanoribbon with its Graphene Nano-Electrodes," Nanoscale, **8**(17), pp. 9265-9271.

[25] Soler, J. M., Artacho, E., Gale, J. D., García, A., Junquera, J., Ordejón, P., and Sánchez-Portal, D., 2002, "The SIESTA Method for Ab Initio Order-N Materials Simulation," Journal of Physics: Condensed Matter, **14**(11), pp. 2745-2780.

[26] Perdew, J. P., Burke, K., and Ernzerhof, M., 1996, "Generalized Gradient Approximation Made Simple," Physical Review Letters, **77**(18), pp. 3865-3868.

[27] Artacho, E., Sánchez-Portal, D., J., Ordejón, P., García, A., and Soler, J. M., 1999, "Linear-Scaling Ab-Initio Calculations for Large and Complex Systems," Physica Status Solidi (B), **215**(1), pp. 809-817.

[28] Bonardi, P., Achilli, S., Tantardini, G. F., and Martinazzo, R., 2015, "Electron Transport in Carbon Wires in Contact with Ag Electrodes: A Detailed First Principles Investigation," Physical Chemistry Chemical Physics, **17**(28), p. 18413.

[29] Matsuda, Y., Tahir-Khell, J., and Goddard, W. A., III., 2010, "Definitive Band Gaps for Single- Wall Carbon Nanotubes," Journal of Physical Chemistry Letters, **1**(19), pp. 2946-2950.

[30] The Siesta Group, 2016, "USER'S GUIDE: SIESTA 4.0," Retrieved from https://departments.icmab.es/leem/siesta/Documentation/Manuals/siesta-4.0.pdf

[31] Band, Y. B., and Avishai, Y., 2013, *Quantum Mechanics with Applications to Nanotechnology and Information Science*, Academic Press, Amsterdam, The Netherlands, Chap. 13, p. 757.

[32] Brandbyge, M., Mozos, J., Ordejón, P., Taylor, J., and Stokbro, K., 2002, "Density-Functional Method for Nonequilibrium Electron Transport," Physical Review B, **65**(16), p. 165401.

[33] Meija, J., Coplen, T., Berglund, M., Brand, W. A., De Bièvre, P., Gröning, M., Holden, N. E., Irrgeher, J., Loss, R. D., Walczyk, T., and Prohaska, T., 2016, "Atomic Weights of the Elements 2013 (IUPAC Technical Report)," Pure and Applied Chemistry, **88**(3), pp. 265-291.

[34] Sun, G., K urti, J., Kertesz, M., and Baughman, R. H., 2003, "Variations of the Geometries and Band Gaps of Single-Walled Carbon Nanotubes and the Effect of Charge Injection," Journal of Physical Chemistry, **107**(29), pp. 6924-6931.

[35] Rabiee Golgir, H., Faez, R., Pazoki, M., Karamitaheri, H., and Sarvari, R., 2011, "Investigation of Quantum Conductance in Semiconductor Single-Wall Carbon Nanotubes: Effect of Strain and Impurity," Journal of Applied Physics, **110**(6), p. 064320.

[36] Thomsen, C., Reich, S., and Maultzsch, J., 2004, *Carbon Nanotubes: Basic Concepts and Physical Properties*, Wiley-VCH Verlag GmbH, Weinheim, Germany, Chap. 5, p. 86.

[37] Cambré, S., Wenseleers, W., Goovaerts, E., and Resasco, D. E., 2010, "Determination of the Metallic/Semiconducting Ratio in Bulk Single-Wall Carbon Nanotube Samples by Cobalt Porphyrin Probe Electron Paramagnetic Resonance Spectroscopy," ACS Nano, **4**(11), pp. 6717-6724.

[38] Buia, C., Buldum, A., and Lu, J. P., 2003, "Quantum Interference Effects in Electronic Transport through Nanotube Contacts," Physical Review B, **67**(11), p. 113409.

[39] Bell, R. A., 2015, *Conduction in Carbon Nanotube Networks*, Springer, Cham, Switzerland, Chap. 2, p. 14.

[40] Saito, S., 1999, "Design of Fullerene-Based Solids and Fullerides, Fullerenes, Kadish, K. M., and Ruoff, R. S., 1^{st} ed., Vol. **4** *Recent Advances in the Chemistry and Physics of Fullerenes and Related Materials*, The Electrochemical Society, New Jersey, USA, pp. 1055-1062.

[41] Matula, R. A., 1979, "Electrical Resistivity of Copper, Gold, Palladium, and Silver," Journal of Physical and Chemical Reference Data, **8**(4), p. 1147.

[42] Mann, D., Javey, A., Kong, J., Wang, Q., and Dai, H., 2003, "Ballistic Transport in Metallic Nanotubes with Reliable Pd Ohmic Contacts," Nano Letters, **3**(11), pp. 1541-1544.

[43] Tison, Y., Giusca, C. E., Stolojan, V., Hayashi, Y., and Silva, S. R. P.,

2007, "The Inner Shell Influence on the Electronic Structure of Double-Walled Carbon Nanotubes," Advanced Materials, **20**(1), pp. 189-193.